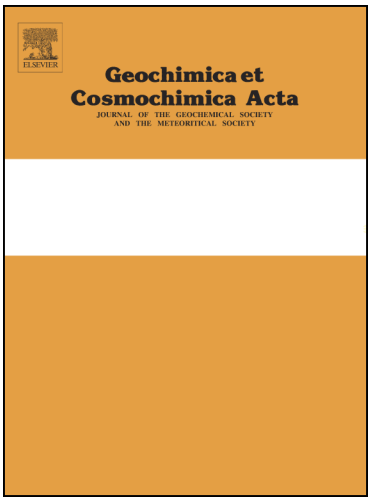

Coupled evolution of nitrogen cycling and redoxcline dynamics on the Yangtze Block across the Ediacaran-Cambrian transition

Yan Chen, Charles W. Diamond, Eva E. Stüeken, Chunfang Cai, Benjamin C. Gill, Feifei Zhang, Steve M. Bates, Xuelei Chu, Yi Ding, Timothy W. Lyons

PII: S0016-7037(19)30284-4
DOI: https://doi.org/10.1016/j.gca.2019.05.017
Reference: GCA 11243

To appear in: *Geochimica et Cosmochimica Acta*

Received Date: 6 April 2018
Revised Date: 22 April 2019
Accepted Date: 12 May 2019

Please cite this article as: Chen, Y., Diamond, C.W., Stüeken, E.E., Cai, C., Gill, B.C., Zhang, F., Bates, S.M., Chu, X., Ding, Y., Lyons, T.W., Coupled evolution of nitrogen cycling and redoxcline dynamics on the Yangtze Block across the Ediacaran-Cambrian transition, *Geochimica et Cosmochimica Acta* (2019), doi: https://doi.org/10.1016/j.gca.2019.05.017

Coupled evolution of nitrogen cycling and redoxcline dynamics on the Yangtze Block across the Ediacaran-Cambrian transition

Yan Chen [a,b,c,d], Charles W. Diamond [b], Eva E. Stüeken [e,f], Chunfang Cai [a,c,d,*], Benjamin C. Gill [g], Feifei Zhang [h], Steve M. Bates [b], Xuelei Chu [c,d], Yi Ding [a,c,d], Timothy W. Lyons [b,*]

*corresponding author.
E-mail addresses: cai_cf@mail.iggcas.ac.cn (C.F. Cai), timothy.lyons@ucr.edu (T.W. Lyons)

[a] *Key Laboratory of Petroleum Resource Research, Institute of Geology and Geophysics, Chinese Academy of Sciences, Beijing 100029, China*
[b] *Department of Earth Sciences, University of California, Riverside, CA 92521, USA*
[c] *College of Earth and Planetary Sciences, University of Chinese Academy of Sciences, Beijing 100049, China*
[d] *Institution of Earth Science, Chinese Academy of Sciences, Beijing 100029, China*
[e] *University of St Andrews, School of Earth and Environmental Sciences, St Andrews, Fife KY16 9AL, Scotland, UK*
[f] *NASA Astrobiology Institute, Virtual Planetary Laboratory, Seattle, WA 98195, USA*
[g] *Department of Geosciences, Virginia Polytechnic Institute and State University, Blacksburg, VA 24061, United States*
[h] *School of Earth and Space Exploration, Arizona State University, Tempe 85287, USA*

Abstract

The Ediacaran-Cambrian transition is characterized by the evolution of complex eukaryotes and rapid diversification of metazoans. However, linkages between environmental triggers and evolutionary patterns remain unclear. Here, we present high-resolution records of carbon and nitrogen isotopic data ($\delta^{13}C$, $\delta^{15}N$) for a drill core extending from the early Ediacaran Doushantuo Formation to the early Cambrian Jiumenchong Formation, located on the slope of the Yangtze Block. Our data show that sedimentary bulk nitrogen isotope values ($\delta^{15}N_{bulk}$) decrease progressively from the early Ediacaran to the early Cambrian, broadly concurrent with nitrogen isotope data from other sections throughout the Yangtze Block. During the early Ediacaran, however, $\delta^{15}N_{bulk}$ values from our study are higher (maximum 11.2‰) compared to those from more restricted coeval sections, suggesting a higher degree of denitrification in our slope section. The early Ediacaran $\delta^{15}N_{bulk}$ data from the Yangtze Block may thus provide indirect evidence for an upwelling system that led to a shallower redoxcline in slope environments of the Upper Yangtze region. Widespread light $\delta^{15}N_{bulk}$ values from the early Cambrian (minimum −7.5‰) paired with excess silicate-bound nitrogen throughout much of the Yangtze Block are most parsimoniously interpreted as non-quantitative assimilation of ammonium (NH_4^+) with relatively high concentrations of NH_4^+ accumulating in the deep basin. Overall, the spatial and temporal trends in nitrogen cycling across the Yangtze Block suggest that fixed nitrogen was more bioavailable in the Ediacaran-Cambrian Yangtze Basin compared to previously studied Mesoproterozoic sections, although nitrogen speciation in the photic zone may have varied with time. Environmental factors such as oxygen levels and nitrogen bioavailability may have shaped the evolutionary trajectory of life on the Yangtze Block and potentially elsewhere across the Ediacaran-Cambrian transition.

Keywords: Ediacaran; Cambrian; Yangtze Block; Nitrogen cycling; Redoxcline; Ammonium

1. Introduction

The Ediacaran and Cambrian periods, 635 to 485 million years ago (Ma), witnessed the origination and diversification of animal phyla (Brasier, 1979; Shu et al., 2014) and were marked by unusual paleoenvironmental conditions (Brasier, 1992; Schröder and Grotzinger, 2007), including the aftermath of the last snowball Earth glaciation (Halverson et al., 2005; Halverson et al., 2007; Hoffman et al., 2017), and ongoing major tectonic reorganization with the generation of many shallow epeiric seas at low paleolatitudes (Campbell and Allen, 2008). This interval also left indications of increasing oxygen levels in the ocean and atmosphere commonly referred to as the Neoproterozoic Oxygenation Event (NOE; Canfield, 2005; Holland, 2006; Och and Shields-Zhou, 2012). Rising oxygen levels in shallow waters could have facilitated major biological innovations through the expansion of stably oxygenated habitats (e.g., Berkner and Marshall, 1965; Catling et al., 2005) and feedbacks associated with nutrient cycling (e.g., Reinhard et al., 2016; Robbins et al., 2016). According to some studies, the deep ocean was ventilated for the first time in Earth history from the middle of the Ediacaran (~580 Ma) onwards (Fike et al., 2006; Canfield et al., 2007; Johnston et al., 2012). However, other datasets suggest that ocean ventilation occurred transiently over short time scales and did not affect the entire ocean (Canfield et al., 2008; Kendall et al., 2015b; Sperling et al., 2015; Sahoo et al., 2016). Widespread ventilation of the deep ocean may not have occurred until later in the Paleozoic with the ecological expansion of land plants (Dahl et al., 2010; Saltzman et al., 2011; Sperling et al., 2015; Lenton et al., 2016; Wallace et al., 2017).

While oxygen is an essential energy source in the metabolism of macroscopic metazoans (Catling et al., 2005), other nutrients would also have been required for the proliferation of complex life (Moore et al., 2013; Knoll, 2017). Experimental and modeling studies have suggested that an increase in nutrient availability, fixed nitrogen for instance, could have supported larger primary producers, such as eukaryotic algae (e.g. Ward et al., 2014), which could in turn have driven increasing ecosystem complexity (Knoll and Follows, 2016). Eukaryotic organisms, including algae and animals, are unable to metabolize atmospheric N_2 and therefore depend on a constant supply of fixed nitrogen (Lindell and Post, 1995; Falkowski, 1997; Tyrrell, 1999; Canfield et al., 2010). Assessing nitrogen bioavailability in Neoproterozoic habitats is therefore critical to understanding the drivers of early animal evolution.

Nitrogen isotope data—expressed as $\delta^{15}N = [(^{15}N/^{14}N)_{sample} / (^{15}N/^{14}N)_{air} - 1] \times 1000$—are the primary tool used for reconstructing nitrogen cycling in ancient and modern environments. These data can also contain information about local redox processes because nitrogen is a redox sensitive element. Multiple studies have investigated variations in bulk sedimentary nitrogen isotope values ($\delta^{15}N_{bulk}$) during the Ediacaran-early Cambrian transition, including in South China where a thick and relatively continuous succession across this time interval is preserved (Cremonese et al., 2013a; Cremonese et al., 2013b; Wang and Zhang, 2013; Ader et al., 2014; Kikumoto et al., 2014; Cai et al., 2015; Wang et al., 2015; Hammarlund et al., 2017; Wang et al., 2017; Wei et al., 2017; Zhang et al., 2017; Li et al., 2018; Wang et al., 2018a; Wang et al., 2018b; Xiang et al., 2018). In general, these studies show a decrease in $\delta^{15}N_{bulk}$ values from the early Ediacaran to early Cambrian. High $\delta^{15}N_{bulk}$ values in the Ediacaran have been interpreted to reflect incomplete denitrification (Cremonese et al., 2013b; Kikumoto et al., 2014; Hammarlund et al., 2017; Wang et al., 2017; Wei et al., 2017; Xiang et al., 2018) and oxygenation of deep water (Ader et al., 2014; Wang et al., 2018a; Wang et al., 2018b), and the low average $\delta^{15}N_{bulk}$ values in the early Cambrian have been interpreted as evidence of N_2-fixation and non-quantitative ammonium (NH_4^+) assimilation resulting from anoxia in the photic zone (Cremonese et al., 2013b; Cai et al., 2015; Wang et al., 2015; Wei et al., 2017; Zhang et al., 2017; Li et al., 2018; Wang et al., 2018a).

However, oxygenation of deep waters in the Yangtze basin during the Ediacaran-Cambrian transition seems contradictory to the local redox scenario posed by trace metal abundance and isotope data (e.g., Kendall et al., 2015a; Sahoo et al., 2016; Dahl et al., 2017; Xiang et al., 2017), iron speciation data (e.g., Canfield et al., 2008; Li et al., 2010; Sperling et al., 2015), and sulfur isotope data (e.g., Mcfadden et al., 2008; Feng et al., 2014), which suggest that while the deep ocean may have experienced temporary oxygenation events, the longer-term average conditions were characterized by predominantly anoxic and iron-rich (ferruginous) deep waters with sulfidic (euxinic) conditions present along productive margins. In order to reconcile these observations with the $\delta^{15}N$ record, a high-resolution, spatially-resolved picture of basinal $\delta^{15}N$ values is essential. To further our understanding, we have analyzed samples at high stratigraphic resolution from a drill core (zk2012) that provides a relatively continuous record of mid-slope depths on the Yangtze block from the basal Ediacaran through early Cambrian Stage 3 and report new organic carbon isotope ($\delta^{13}C_{org}$) and bulk $\delta^{15}N$ values. In conjunction with published data, we explore spatial and temporal trends in nitrogen isotope values across the Yangtze Block to unravel possible links between nitrogen availability, water-column redox, and biological evolution during the Ediacaran and early Cambrian.

2. Background

2.1. The oceanic nitrogen cycle

The most significant nitrogen reservoir at Earth's surface and the ultimate source of nitrogen for the biosphere is atmospheric N_2. The principal source of nitrogen to the ocean is biological N_2-fixation, where atmospheric N_2 is converted enzymatically to bioavailable NH_4^+. The largest sinks for fixed nitrogen in the ocean are denitrification and anaerobic ammonium oxidation (anammox), which ultimately return nitrogen as N_2 to the atmosphere (e.g. Sigman et al., 2009). Deposition of organic nitrogen into sediments is considered a minor sink for oceanic fixed nitrogen, which can be balanced by inputs from volcanism and weathering over geologic timescales (Mather et al., 2004; Berner, 2006; Canfield et al., 2010). The major chemical species of fixed nitrogen in seawater are nitrate (NO_3^-) under oxic conditions and NH_4^+ under anoxic conditions. The fixed nitrogen reservoir in the modern ocean is dominantly NO_3^- with a $\delta^{15}N_{NO3-}$ value of ~5‰, an average concentration of ~30 μM at depth, and a residence time of slightly less than 2000 years—1.5 to 2 times greater than the mixing time of the oceans (Brandes and Devol, 2002; Sigman et al., 2009).

Biological N_2-fixation, the assimilation of molecular N_2 into organic matter, is an energetically costly process that is performed by a select group of prokaryotes (mainly cyanobacteria today). It dominates the ecosystem when bioavailable nitrogen limits primary production (Karl et al., 2002; Sohm et al., 2011). Nitrogen fixation (diazotrophy) with the most common nitrogenase enzyme (Nif, with Mo and Fe as cofactors) imparts a small isotopic fractionation of −1‰ on average ($\varepsilon_{product\text{-}reactant}$ = −2‰ to 1‰), with an exception under Fe^{2+}-rich conditions or in thermophilic cultures where fractionations can be as large as −4‰ (Zerkle et al., 2008; Nishizawa et al., 2014; Zhang et al., 2014). The Black Sea is a modern example where N_2-fixation is the major pathway of nitrogen acquisition, and sedimentary $\delta^{15}N$ values range from −2‰ to 1‰ (Fulton et al., 2012). Assuming that the isotopic composition of atmospheric N_2 has remained close to 0‰ over Earth's history (Sano and Pillinger, 2008), $\delta^{15}N$ values between −4‰ and 1‰ in ancient sedimentary rocks (most commonly −2‰ to 1‰) are typically attributed to a nitrogen cycle dominated by anaerobic N_2-fixation (Fig. 1). Alternative nitrogenase enzymes, using V and Fe as cofactors, can induce larger isotopic fractionations (−6‰ to −8‰; Zhang et al., 2014) (Fig. 1). Such light values, however, are rare in the geologic record, suggesting that the Mo-based enzyme has been the dominant means of N_2-fixation throughout geological history (Stüeken et al., 2016).

Other pathways for biological N acquisition are direct assimilation of NO_3^- and NH_4^+. Many prokaryotic and eukaryotic organisms can assimilate NH_4^+, but incomplete assimilation imparts large nitrogen isotopic fractionations in resulting biomass, ranging from −4‰ to −27‰ depending on ambient NH_4^+ concentrations (Hoch et al., 1992; Pennock et al., 1996; Vo et al., 2013) (Fig. 1). Nitrate assimilation can also result in fractionations of −5‰ to −10‰ (Fig. 1; Casciotti, 2009). However, neither of these fractionations is expressed during quantitative assimilation, which is the case in most of the modern ocean apart from high latitude eutrophic areas and the Pacific equatorial upwelling system (Altabet and Francois, 1994; Sigman et al., 2009). Hence, the isotopic composition of sedimentary rocks containing ancient biomass is often assumed to approximate the isotopic composition of the major coeval nitrogen metabolite, except under very high nitrogen supplies (Sigman et al., 2009; Ader et al., 2016; Stüeken et al., 2016).

When primary producers die, their bound N can be remineralized to NH_4^+ with minimal fractionation (Prokopenko et al., 2006). In the presence of free oxygen, NH_4^+ is rapidly oxidized to nitrite (NO_2^-) (ε = 14‰ to 38‰; Casciotti et al., 2003) and then NO_3^- (ε = −13‰; Casciotti, 2009) through a process called nitrification (Fig. 1). Although individual steps in nitrification are associated with large fractionations, there is typically no net isotopic effect because nitrification is rapid even under micromolar levels of dissolved oxygen, and thus the process is typically quantitative (Lipschultz et al., 1990). In rare cases where nitrification does not go to completion, evidence for it can be expressed as large scatter of positive $\delta^{15}N$ values in sediments (Granger et al., 2011).

Denitrification and anammox are two major sinks for oceanic fixed nitrogen. Both processes are carried out under suboxic conditions and occur today mostly in oxygen minimum zones and sediment pore waters (Prokopenko et al., 2006; Lam et al., 2009; Sigman et al., 2009). The isotopic fractionation effect of denitrification in water is around −25‰ with the residual NO_3^- pool enriched in the heavier ^{15}N, whereas in sediments the net isotopic effect is hardly discernable (Fig. 1; Sigman et al., 2009; Devol, 2015). The isotopic fractionation of anammox, where denitrification is coupled to oxidation of NH_4^+, is similar to that of denitrification in water (Fig. 1; Brunner et al., 2013). In oxygen minimum zones and sediments, NO_3^- can also be reduced to NH_4^+ instead of N_2 via dissimilatory nitrate reduction to ammonium (DNRA; Sørensen, 1978; Kartal et al., 2007; Lam et al., 2009). The isotopic effect of DNRA is likely similar to denitrification and anammox, with residual NO_3^- becoming isotopically heavier (Fig. 1; McCready et al., 1983). The NH_4^+ that results from DNRA can then be subject to anammox, nitrification, biological assimilation, or adsorption onto clay particles. Importantly, all three NO_3^--reducing

pathways (denitrification, anammox, and DNRA) render the residual NO_3^- pool isotopically heavy—a signature that can be preserved in biomass assimilating NO_3^- if the reduction is non-quantitative.

2.2. Geological setting

The South China craton consists of the Yangtze and Cathaysia blocks. These two blocks merged around 870 Ma (Li et al., 2008; Charvet, 2013). Beginning at ~800 Ma, with the breakup of Rodinia, a rift developed between the Yangtze and Cathaysia blocks, although the two remained close, merging once again in the early Paleozoic (Charvet, 2013). The South China craton as a whole broke free from Rodinia and, according to paleomagnetic studies, drifted from ~30°N in the mid-Neoproterozoic to equatorial latitudes by the early Cambrian (Fig. 2A; Jiang et al., 2003; Zhang et al., 2015). During the mid-late Neoproterozoic, the basin between the Yangtze Block and the Cathaysia Block evolved from active rifting to a passive continental margin (Wang and Li, 2003; Li et al., 2008). It can be inferred that the basin was connected to the open ocean from the mid-Neoproterozoic to the early Cambrian based on the presence of globally distributed marine fossils (Zhou et al., 2007; Liu et al., 2013).

The Yangtze Block holds one of the world's most complete records of Neoproterozoic through Ordovician strata. Over this time, sedimentation occurred broadly on rimmed shallow platforms to the present-day northwest and along a deep basin to the southeast (Chen et al., 2009; Jiang et al., 2011). The marginal zone of the Yangtze platform extended southwest-northeast, approximately along the trend of the earlier Jiangnan orogeny, as the basin was created largely through rifting of the Yangtze and Cathaysia blocks (Fig. 2B; Zheng et al., 2008; Jiang et al., 2011). During the early Cambrian, the carbonate platforms in the northwest portion of the block suffered widespread drowning as a consequence of rapid sea level rise (Goldberg et al., 2007).

Our studied drill core (zk2012) was taken in the eastern portion of the Guizhou Province, South China. At the time of deposition, this location was situated on the slope of the Yangtze platform among multiple topographic highs and sub-basins (Fig. 2B). The studied core preserves a relatively continuous record from the early Ediacaran to Cambrian Series 2 (Fig. 2C). The drill core intersects, in ascending order, the Doushantuo, Liuchapo, and Jiumenchong formations. The Doushantuo Formation (~95 m) consists of four widely recognized members. The oldest of the four, Member I, is a ~5 m 'cap carbonate' that overlies the Nantuo glacial diamictite. The contact between the Nantuo and Doushantuo formations marks the end of the

Cryogenian and the beginning of the Ediacaran period at ~635 Ma (Condon et al., 2005; Jiang et al., 2011; Zhou et al., 2019). Above the cap carbonate, Member II consists of laminated black shales with rare interbedded carbonates (~20 m). Thick bedded carbonates dominate Member III (~60 m). Member IV (~10 m) is defined by a return to shale deposition and is composed of organic rich, phosphatic shales that serve as an important regional marker bed in the Yangtze region (Zhu et al., 2003). Some workers have identified a disconformity at the contact of members III and IV, although it is not clear that this hiatus was regional in extent or how much time may be missing (Zhu et al., 2007b; Jiang et al., 2011).

Member IV of the Doushantuo Formation is overlain by a thin (~0.4 m) phosphorite bed that marks the base of the Liuchapo Formation. The ~35-m-thick Liuchapo Formation is composed mainly of bedded cherty shale with phosphatic cherty shale and phosphate nodules present at the top. The overlying Jiumenchong Formation, the lower 45 m of which was sampled, is mainly composed of carbonaceous black shale. A horizon enriched in Ni–Mo–PGE, sulfide, and phosphate (~6 m) is present in the lower part of Jiumenchong Formation. The Ni–Mo–PGE-rich bed can be used as a correlation marker across the margin of the Yangtze platform (Zhu et al., 2003; Jiang et al., 2012). For this study, we targeted siliciclastic facies; pure carbonates were not sampled.

2.3. Regional stratigraphic correlation

To correlate the regional stratigraphy across the Yangtze Block, biostratigraphy, carbon isotope stratigraphy, and lithostratigraphic markers such as the Ni–Mo–PGE sulfide layer and horizons of phosphatic nodules (described below) can be used in combination with geochronologic data. The strata of Ediacaran and early Cambrian age from the slope-basinal facies on the Yangtze Block contain few fossils (including our studied core), presenting a challenge for high-resolution biostratigraphic correlation (e.g. Yuan et al., 2014; Cai et al., 2015; Wang et al., 2015; Jin et al., 2016; Wang et al., 2018a). However, a broad correlation can be established with the use of shared marker beds, carbon isotope excursions and geochronologic data as presented by previous studies (e.g. Yuan et al., 2014; Cai et al., 2015; Chen et al., 2015a; Wang et al., 2015; Jin et al., 2016; Wang et al., 2018a). Here, we have followed the same correlation principle and adopted the general stratigraphic correlation that has been employed by numerous previous studies (e.g. Yuan et al., 2014; Cai et al., 2015; Chen et al., 2015a; Wang et al., 2015; Jin et al., 2016; Wang et al., 2018a).

The Doushantuo Formation in the studied drill core is characterized by a cap carbonate at the bottom and a black shale

succession at the top that serve as marker beds and can be correlated with equivalent units in the Yangtze Gorges area (Figs. 3, and 5; Jiang et al., 2011; Zhou et al., 2019). The age of the Doushantuo Formation is constrained by radiometric dates of 634.57 ± 0.88 Ma at the base of the formation (Zhou et al., 2019) and 551 ± 0.7 Ma at the top (Fig. 4; Condon et al., 2005), suggesting a duration of deposition on the order of ~84 Ma. The overlying Liuchapo Formation is generally considered to be a diachronous stratigraphic unit that includes the upper part of the Ediacaran and likely the lowest Cambrian in our core (Figs. 3, 4, and 5; e.g. Chen et al., 2015a; Wang et al., 2018a). The shallow-water equivalents to the Ediacaran portion of the Liuchapo Formation are the carbonate deposits of the Dengying Formation (e.g. Jin et al., 2016), while the deep-water equivalents in the lower Yangtze region are the chert and shale deposits of the Piyuancun Formation (Figs. 4, and 5; Yang et al., 2003; Zhu et al., 2003; Yang et al., 2008).

A U-Pb age of 541.00 ± 0.13 Ma—generally accepted as the base of the Cambrian—was obtained from Oman for the globally recognizable basal Cambrian negative carbon isotope excursion (BACE) (Bowring et al., 2007; Maloof et al., 2010). For sections deposited on the shallow Yangtze Platform, an unconformity and/or erosional event can be identified at the top of the Dengying Formations, which broadly corresponds to eustatic regression across the Ediacaran-Cambrian boundary (Jiang et al., 2012). Hence, on the basis of the appearance of small shelly fossil group 1 (e.g., Chen, 1984; Zhou et al., 1997; Li, 2004; Steiner et al., 2007; Guo et al., 2014), $\delta^{13}C$ chemostratigraphy (BACE; e.g., Zhou et al., 1997; Yang et al., 2007; Kikumoto et al., 2014; Wang et al., 2015), and radiometric dating (e.g., Jiang et al., 2009; Zhu et al., 2009; Xu et al., 2011; Chen et al., 2015a), the Ediacaran-Cambrian boundary has been assigned to the contacts between the Dengying and overlying formations (Figs. 4, and 5). For sections deposited in deeper waters without significant occurrence of fossil markers or transformation of lithology, such as the Yuanjia, Yanjia, Lijiatuo, Longbizui, Huanglian/Daotuo sections, and our studied core, the Ediacaran-Cambrian boundary has been placed in the upper part of Liuchapo and Piyuancun formations on the basis of $\delta^{13}C_{org}$ variations (BACE; Guo et al., 2007; Wang et al., 2012a; Cremonese et al., 2013b; Guo et al., 2013; Wang et al., 2015; Wei et al., 2017; Wang et al., 2018a) and radiometric ages (Zhou et al., 2013; Chen et al., 2015a; Yang et al., 2017) (Figs. 3, 4, and 5).

A distinctive Ni–Mo–PGE sulfide-rich phosphatic horizon is present at the base of the Jiumenchong Formation in the studied core and can be correlated with anomalous enrichments in Ni, Mo, and PGEs throughout much of the Yangtze platform and slope near the base of the Niutitang and correlative formations (Zhu et al., 2003; Jiang et al., 2012). Several dates obtained

for the Ni–Mo–PGE horizon and the horizons immediately below it in other sections are within error of 522 Ma (Fig. 4; Xu et al., 2011; Wang et al., 2012b; Chen et al., 2015a), supporting the notion that distinct Ni–Mo–PGE deposits occurred synchronously across the Yangtze Block and are latest Cambrian Stage 2 in age (Figs. 4, and 5; Landing et al., 1998; Steiner et al., 2007; Gradstein et al., 2012). The age of this horizon is also consistent with U-Pb ages in the underlying upper Liuchapo Formation, of 536.3 ± 5.5 Ma in western Hunan (Chen et al., 2009) and of 536 ± 5 Ma in northeastern Guizhou (Figs. 4 and 5; Zhou et al., 2013). At the intrashelf Xiaotan section, the Ni–Mo–PGE sulfide-rich shales can be correlated with a Ni-rich layer in the upper Shiyantou Formation (Och et al., 2013), considering a U-Pb age of 526.5 ± 1.1 Ma at the base of Shiyantou Formation at Meishucun section (Compston et al., 2008) (Figs. 4, and 5). The Ni–Mo–PGE-enriched layer in the Yangtze Gorges composite section is unapparent probably because of an unconformity of unknown duration at the top of Yanjiahe Formation but has been correlated to the base of Shuijingtuo Formation using small shelly fossils (Figs. 4, and 5; Chen, 1984; Steiner et al., 2007).

Given the date of ~522 Ma for Ni–Mo–PGE deposits, the stratigraphic intervals between the Edicaran-Cambrian boundary and the Ni–Mo–PGE deposits across the Yangtze Block belong to Cambrian Fortunian-late Stage 2 (Figs. 4, and 5). The strata from this interval on the slope are thinner than might be expected for ~20 myrs of deposition, including in the studied core where it is a mere ~3 m (Fig. 5). This suggests that there may have been periods of erosion or non-deposition during this interval (Zhu et al., 2003; Steiner et al., 2007; Jiang et al., 2012).

The base of Cambrian Stage 3 is commonly placed at the base of the Yu'anshan Formation at Xiaotan and the base of the Shuijingtuo Formation in the Yangtze Gorges area based on small shelly fossil distributions (Figs. 4, and 5; Zhou et al., 1997; Steiner et al., 2007). Correlation of the base of Cambrian Stage 3 to other sections is difficult because of the lack of fossil markers and other indicators in these sections (Figs. 4, and 5).

3. Materials and methods

3.1. Sample preparation

All sample preparation was carried out at the Biogeochemistry Lab at the University of California, Riverside (UCR). Prior to analyses, core samples were cut with a water-cooled saw to remove outer surfaces. Samples with visible veining and pyrite nodules were avoided. Dry unaltered sample pieces were then pulverized in an alumina ceramic puck mill cleaned with 10%

HCl, methanol, and DI-H_2O after each sample. All subsequent geochemical measurements were carried out on these powders.

3.2. Measurement of total organic carbon, total nitrogen, $\delta^{13}C_{org}$, and $\delta^{15}N_{bulk}$

Total organic carbon (TOC) concentrations were calculated as the difference between total carbon (by combustion) and total inorganic carbon (TIC, by acidification) using standard methods on an Eltra CS-500 carbon/sulfur analyzer at UCR. The analytical reproducibility of TOC and TIC were less than ±0.2% based on repeated analyses of standard materials and samples. Additional determinations of TOC content were carried out along with total nitrogen (TN) analyses on decarbonated samples using methods described in Stüeken (2013) and agree well with values obtained from the Eltra C/S analyzer. In brief, a measured amount of each sample (~0.5 g) was decarbonated with 6M HCl for 2 days; the acid was refreshed each day. The decarbonated samples were then rinsed with DI-H_2O to remove residual acid, dried, homogenized, and weighed. Measurements of TOC and TN concentrations were carried out along with $\delta^{13}C$ and $\delta^{15}N$ in decarbonated samples at Virginia Tech using an Isoprime 100 isotope-ratio mass spectrometer (IRMS) coupled to an Elementar vario Isotope Cube elemental analyzer. Values for $\delta^{15}N_{bulk}$ and $\delta^{13}C_{org}$ are expressed in per mil notation relative to atmospheric N_2 and Vienna PeeDee Belemnite, respectively. Reference materials—acetanilide, urea (Elemental Microanalysis), IAEA CH-6, and IAEA CH-7—were used to calibrate TOC and $\delta^{13}C_{org}$, with precisions (±1σ) of ±0.1‰ for the latter. Based on the TN contents in the first run, a separate run was conducted to analyze for TN and $\delta^{15}N_{bulk}$ with an adjusted sample load to obtain 0.04−0.06 mg nitrogen. Data from this run were calibrated against reference materials—acetanilide, urea (both Elemental Microanalysis), USGS-24, and USGS-26—with isotopic precisions within ±0.2‰.

4. Results

4.1. Core zk2012

Elemental abundances and isotopic data for the Doushantuo, Liuchapo, and Jiumenchong formations are summarized in Fig. 3 and Supplementary Data S1. Concentrations of TOC range from less than 0.1 wt.% to 14.0 wt.%, with an average value for the whole succession of 3.5 ± 3.3 wt.% (n = 150). Two intervals stand out as being more strongly enriched in TOC: one in Member II of the Doushantuo Formation and another that spans the contact between the Liuchapo and Jiumenchong formations. Total nitrogen ranges from 0.0 wt.% to 0.4 wt.%, with an average of 0.1 ± 0.1 wt.% (n = 150), and displays a similar trend to that of TOC (positive correlation, $R^2 = 0.5$ for Jiumenchong and Doushantuo formations, $R^2 = 0.4$ for Liuchapo Formation; Fig. 6a). Atomic C_{org}/N ratios were calculated from TOC and TN concentrations and their respective

molar masses and average 34.9 ± 24.3 (n = 150). Comparatively higher C_{org}/N values are found in the Doushantuo Formation and lower values in Jiumenchong Formation.

The isotopic composition of organic carbon ranges from −37.9‰ to −27.7‰ and averages −33.2 ± 2.0‰ (n = 149), with two conspicuous negative $\delta^{13}C_{org}$ excursions: one in the upper Liuchapo Formation and the other in the middle of the Jiumenchong Formation. The isotopic composition of bulk nitrogen ranges from −2.4‰ to 11.2‰, with an average of 3.2 ± 3.5‰ (n = 88). Average $\delta^{15}N_{bulk}$ values decrease stepwise from the Doushantuo Formation (7.8 ± 2.1‰, n = 16) to the Liuchapo Formation (7.0 ± 1.6‰, n = 14) and again into the Jiumenchong Formation (−0.9 ± 1.6‰, n = 57).

4.2. Nitrogen isotope data from the Yangtze Block

Based on the stratigraphic framework described above, a correlation of $\delta^{15}N_{bulk}$ values across the Yangtze platform and slope is presented in Fig. 5 and Supplementary Data S2. The temporal evolution of $\delta^{15}N_{bulk}$ values captured in the studied drill core and other sections throughout the Yangtze Block can be divided into four intervals (Figs. 5, and 7; Supplementary Data S2): the early Ediacaran, late Ediacaran, Fortunian to late Cambrian Stage 2, and latest Cambrian Stage 2 to Cambrian Stage 3. In general, $\delta^{15}N_{bulk}$ values on the Yangtze Block decrease from the early Ediacaran to the early Cambrian. This regionally consistent pattern further substantiates that variation in $\delta^{15}N_{bulk}$ reflects primary signals rather than post-depositional alteration.

When statistically averaged across the Yangtze Block, $\delta^{15}N_{bulk}$ values are highest in the early Ediacaran, averaging 5.3 ± 1.5‰ (n = 222), and decrease in the late Ediacaran to 3.5 ± 2.7‰ (n = 55). Average $\delta^{15}N_{bulk}$ values continue to decrease into the early Cambrian (Fortunian-late Stage 2; average 2.2 ± 2.1‰, n = 239) and again in latest Stage 2-Stage 3 to the lowest observed average value of 0.6 ± 1.9‰ (n = 267) (Figs. 5, and 7). In the early Ediacaran, $\delta^{15}N_{bulk}$ values range from 2.3‰ to 11.2‰ in the basin, with a 2.7‰ basinal gradient (calculated as the difference between facies averages) from the slope, represented by the studied drill core, to the more restricted waters of the intrashelf Yangtze Gorges composite and Lantian sections. The range of compiled $\delta^{15}N_{bulk}$ values for the late Ediacaran decreases to −1.8‰ to 10.2‰, but a basinal gradient persists (3.0‰), with higher values in offshore sections and lower values on the platform (with the exception of the Yuanjia section). In the Fortunian-late Stage 2 interval, $\delta^{15}N_{bulk}$ values range from −4.3‰ to 8.8‰ and the basinal gradient apparent throughout the Ediacaran was no longer present. In latest Stage 2-Stage 3, $\delta^{15}N_{bulk}$ values begin consistently lower without a

significant spatial gradient (in temporal proximity to the Ni–Mo enriched horizon) but return to relatively higher values upsection in several localities (ranging from −7.5‰ to 6.4‰; Figs. 5, and 7).

5. Discussion

5.1. Evaluation of primary isotopes values

Terrestrial input, diagenesis, metamorphism, and metasomatism can all alter sedimentary $\delta^{15}N_{bulk}$ signals. In order to make reliable biogeochemical interpretations, we first evaluate our data in terms of the processes that can alter $\delta^{15}N_{bulk}$ and $\delta^{13}C_{org}$ values.

Contributions of terrestrial runoff to the sedimentary nitrogen reservoir should be minor because (1) terrestrial organic matter input was limited before the Devonian (Kenrick and Crane, 1997) and (2) our samples were deposited in a distal setting, far from land. Total nitrogen is well correlated with total organic carbon, indicating that most nitrogen came from marine organic matter (Fig. 6a). The positive intercept of 2000 ppm on the TN axis for the Jiumenchong Formation in Fig. 6a, which is not present for the other two formations, indicates the presence of some inorganic clay-bound nitrogen (Calvert, 2004; Bristow et al., 2009). This fraction may reflect detrital input but is probably to a large extent derived from anaerobic remineralization of biomass in sediments where organic carbon escaped as CO_2, while organic nitrogen was trapped as NH_4^+ (discussed further in Section 5.2.4) (Boatman and Murray, 1982; Schroeder and Mclain, 1998). Similar excess N has previously been reported from the Jiumenchong Formation and its stratigraphic equivalents across the Yangtze Block in sections such as Xiaotan, Yangtze Gorges, Sancha, Nangao, Daotuo, Longbizui, Lijiatuo, and Yuanjia (Cremonese et al., 2013a; Cremonese et al., 2013b; Kikumoto et al., 2014; Wang et al., 2015; Wang et al., 2017; Wei et al., 2017; Zhang et al., 2017). A large detrital input of inorganic nitrogen is unlikely because the Jiumenchong Formation has high TOC compared to the other two formations (Fig. 3), and a detrital contribution would represent a larger fraction of the total nitrogen pool when TOC was low. Further, the magnitude of the positive N-intercepts for the Jiumenchong Formation and its stratigraphic equivalents does not change with distance from the continent, supporting the assertion that the excess nitrogen was not sourced from terrestrial runoff.

Although some nitrogen and carbon were probably mobilized during diagenesis, significant isotopic alteration during this process would have been unlikely. Under oxic depositional conditions, $\delta^{15}N_{bulk}$ values can increase by 3–5‰ during

diagenesis (Robinson et al., 2012). Under anoxic diagenetic conditions, however, $\delta^{15}N_{bulk}$ and $\delta^{13}C_{org}$ values can decrease by up to 1‰ and 1.6‰, respectively (Altabet et al., 1999; Freudenthal et al., 2001; Lehmann et al., 2002). Based on substantial coeval Fe-speciation data published from sites throughout the Yangtze slope (e.g. Canfield et al., 2008; Wang et al., 2012a; Feng et al., 2014; Och et al., 2015), the investigated strata were most likely deposited under a persistently anoxic water column, suggesting that isotopic alteration during early diagenesis would have been minimal and that the large temporal and spatial variations in $\delta^{15}N_{bulk}$ on the Yangtze Block (Fig. 5) cannot be explained by this process alone.

Metamorphism can increase C_{org}/N and $\delta^{15}N_{bulk}$ to some extent, with an isotopic effect of 1–2‰ for greenschist facies and 3–4‰ for amphibolite facies (Bebout and Fogel, 1992; Boyd and Philippot, 1998; Mingram and Bräuer, 2001; Thomazo and Papineau, 2013). However, high organic H/C ratios (0.3–1.8; Guo et al., 2007) and low vitrinite reflectance (R_o < 4%; Han et al., 2013; Tan et al., 2015) reported from other sections near our studied drill core suggest that the effects of regional metamorphism are unlikely to be significant (Hayes et al., 1983). Similarly, metamorphic overprints on $\delta^{13}C_{org}$ are considered to be insignificant (< 3‰) below greenschist facies (Hayes et al., 1983). Additionally, we did not observe any petrologic features indicative of metamorphic or metasomatic processes in the core, such as the development of metamorphic fabrics, shearing, or significant veining.

Additional lines of evidence argue against significant secondary alteration of $\delta^{15}N_{bulk}$ and $\delta^{13}C_{org}$ values in the studied samples. Thermal alteration due to metamorphism tends to result in a preferential loss of ^{14}N and ^{12}C and thus in positive covariance between $\delta^{15}N_{bulk}$ and $\delta^{13}C_{org}$ values (Hayes et al., 1983; Bebout and Fogel, 1992; Ader et al., 1998; Jia, 2006). Similarly, this process should result in covariation between $\delta^{15}N_{bulk}$ and TN (or C_{org}/N). However, there is no obvious correlation in cross plots of $\delta^{15}N_{bulk}$ versus TN and $\delta^{15}N_{bulk}$ versus C_{org}/N for different lithologies and/or formations (Figs. 6b, and 6c). Also, cross plots of $\delta^{15}N_{bulk}$ versus TOC and $\delta^{15}N_{bulk}$ versus $\delta^{13}C_{org}$ do not show significant correlation (Figs. 6d, and 6e). The absence of covariance between any of these parameters argues against a significant metamorphic control on the data. Moreover, almost all the C_{org}/N ratios from the studied drill core are less than 100 (3.1–114; Fig. 3), consistent with the range of Proterozoic C_{org}/N ratios from other settings with little or no metamorphic overprint (Beaumont and Robert, 1999). Although C_{org}/N ratios generally increase in older, sub-greenschist rocks over geologic time, $\delta^{15}N_{bulk}$ values do not increase correspondingly, suggesting that this gradual loss of N does not impart a significant isotopic fractionation if the metamorphic grade is low (Stüeken et al., 2016). In sum, measured $\delta^{13}C_{org}$ and $\delta^{15}N_{bulk}$ values are not likely to have been significantly

altered by post-depositional processes and are likely within 3‰ and 1‰, respectively, of primary signals.

5.2. Nitrogen cycling on the Yangtze Block during the Ediacaran-Cambrian transition

In the modern ocean, large-scale (>100 km) differences in seafloor $\delta^{15}N_{bulk}$ values have been shown to reflect the dominant nitrogen metabolisms in the overlying water column (Tesdal et al., 2013). Over geologic time, sedimentary $\delta^{15}N_{bulk}$ values should reflect the isotopic balance between different nitrogen sources to local biomass—biological N_2-fixation and bioavailable nitrogen sourced through upwelling (NO_3^- and NH_4^+) (Fig. 1; Altabet et al., 2002; Sigman et al., 2009; Ader et al., 2016). Building from the biogeochemical pathways and associated fractionations discussed in Section 2.1, Table 1 presents a summary of dominant nitrogen metabolisms for possible $\delta^{15}N_{bulk}$ distributions in modern and ancient environments. Apart from the mechanism of NH_3 volatilization that has been reported in modern and ancient alkaline lakes (Stüeken et al., 2015; Stüeken et al., 2016), which are markedly different from the open marine environment represented by the Yangtze platform and basin (Fig. 2), various metabolic processes and their implications are considered in detail below.

5.2.1. The early Ediacaran

Compared to the younger units, $\delta^{15}N_{bulk}$ values from the early Ediacaran on the Yangtze Block are on average the highest observed (5.3 ± 1.5‰; Figs. 5, and 7). Our data show for the first time that significantly higher values are present on the slope of Upper Yangtze during this interval (7.8 ± 2.1‰). Lower values are present in the intrashelf Yangtze Gorges (4.7 ± 1.7‰; (Kikumoto et al., 2014) and Lower Yangtze Lantian sections (5.3 ± 1.1‰; (Wang et al., 2017). Such positive $\delta^{15}N_{bulk}$ values (> 2‰) can be attributed to one of three processes in the marine nitrogen cycle (Table 1; Stüeken, 2013; Tesdal et al., 2013; Ader et al., 2016; Stüeken et al., 2016):

(i) Partial nitrification can produce heavy residual NH_4^+ and light NO_3^- in slightly oxygenated surface water. Quantitative assimilation of the isotopically enriched NH_4^+ could then generate positive $\delta^{15}N_{bulk}$ values in biomass and sediments as long as the isotopically light NO_3^- is converted to N_2 via complete denitrification (Thomazo et al., 2011). Today, nitrification goes to completion rapidly in the suboxic zone of the Black Sea and in OMZs along productive margins (Fuchsman et al., 2008; Fussel et al., 2012). Incomplete nitrification has only been reported from the Bering Sea due to seasonally variable oxygen concentrations and results in a large scatter of organic $\delta^{15}N$ values from 2‰ to 18‰ (Granger et al., 2011; Morales et al., 2014). In this scenario, heavy NH_4^+ can be returned to the water column through

organic matter remineralization, resulting in further isotopic fractionation if partial nitrification continues (Stüeken, 2013). This cycle can thus lead to an isotopic imbalance, generating very positive $\delta^{15}N_{bulk}$ values (in excess of 20‰; Morales et al., 2014), which are not observed in the Ediacaran of South China. Assuming the fractionation of nitrification is –25‰, average $\delta^{15}N_{bulk}$ values of 5‰ in the early Ediacaran on the Yangtze Block would suggest nitrification of ~24% of the dissolved NH_4^+. The sink for the residual ~76% of isotopically enriched NH_4^+ would then need to have been biological uptake, which represents a very small sink for fixed N in the modern ocean (Section 2.1).

Alternatively, if partial nitrification were followed by quantitative assimilation by biomass, both the isotopically enriched and depleted phases would be preserved. However no samples on the Yangtze Block exhibit $\delta^{15}N_{bulk}$ values lighter than –2‰ (Kikumoto et al., 2014; Wang et al., 2018b) (Fig. 5). In sum, partial nitrification does not explain the Ediacaran $\delta^{15}N_{bulk}$ from South China.

(ii) Incomplete assimilation of nitrogen (NO_3^- and in particular NH_4^+) may generate a heavy residual nitrogen pool (> 1‰) as biomass preferentially assimilates the light isotope (< –2‰) (Papineau et al., 2009). This process occurs today most conspicuously in high latitude settings and equatorial upwelling zones where the supply of NO_3^- is very high (Tesdal et al., 2013). As the Yangtze Block moved towards the Equator during the Ediacaran (Fig. 2a), it is conceivable that upwelling could have delivered abundant nutrients to the euphotic zone, which could have led to partial uptake of nitrogen by primary producers. However, of the three early Ediacaran datasets, none contain $\delta^{15}N$ values lower than that which could be attributed to N_2-fixation (min. 2.3‰ in the more proximal Three Gorges section; Kikumoto et al., 2014). If partial assimilation generated the heavy $\delta^{15}N$ values reported in our samples, a significant amount of ^{15}N depleted NH_4^+ would need to have been sequestered elsewhere in the basin. While it is not possible to entirely rule this out, we do not find it to be the most parsimonious interpretation.

(iii) Incomplete denitrification, DNRA, or anammox can convert NO_3^- into N_2 or N_2O at the oxic/suboxic interface in physically stratified systems or modern oxygen minimum zones, producing large isotopic fractionations (Kuypers et al., 2003; Gaye-Haake et al., 2005; Kuypers et al., 2005; Sigman et al., 2009). This mechanism generates isotopically heavy NO_3^- in the modern ocean, and the same process could have occurred in the redox-stratified ocean of the early Ediacaran (e.g., Bowyer et al., 2017), with one important difference being that NO_3^- would have been present only in the oxic

surface ocean and not in anoxic deeper waters (e.g., Fig. 1b in Ader et al., 2014) (Fig. 9). The NO_3^- reservoir—established by aerobic degradation of biomass in shallow waters—could have been subject to partial reduction through contact with upwelling anoxic waters. Biomass assimilating the residual NO_3^- in the photic zone could have acquired the isotopic signature deriving from this partial NO_3^- reduction. The NO_3^- would not necessarily be completely depleted by denitrification or anammox if the chemocline was relatively deep, particularly below the photic zone—sources and sinks in the surface NO_3^- reservoir could have been balanced, similar to conditions found today in the Cariaco Basin where the nitrate maximum is ~10-15 μM in the surface water (Ho et al., 2004) and the redoxcline is situated at ~275 m (Thunell et al., 2004).

In modern oxygen minimum zones, where a significant amount of fixed nitrogen is lost via denitrification and anammox (Lam et al., 2009; Dalsgaard et al., 2012), the highest $\delta^{15}N_{bulk}$ values occur in the core of the OMZ where the degree of NO_3^- reduction is highest (Sigman et al., 2009; Tesdal et al., 2013). A similar scenario could explain the strong basinal heterogeneity in sedimentary $\delta^{15}N_{bulk}$ values in the early Ediacaran of the Yangtze Block (Figs. 5, 7a, and 9), although NO_3^- would have been sourced from the surface rather than from upwelling anoxic deep waters. Specifically, the extremely high $\delta^{15}N_{bulk}$ values (up to 11.2‰) on the slope of the Upper Yangtze, compared to the more "normal-marine" $\delta^{15}N_{bulk}$ values in the intrashelf basin and Lower Yangtze region, may reflect an upwelling system and more intense denitrification on the slope—the surface NO_3^- reservoir being most strongly depleted there due to reaction with upwelling reductants. It is also possible that upwelling along the slope supplied nutrients locally and resulted in higher primary and export production compared to the intrashelf basin and Lower Yangtze. This would have also contributed to an elevated redoxcline and a higher degree of NO_3^- reduction. Higher TOC values on the slope support this possibility (Fig. 3) (Kikumoto et al., 2014).

However, even with intense denitrification leading to severe loss of fixed nitrogen, the preservation of high $\delta^{15}N_{bulk}$ in sediments implies that there was still sufficient NO_3^- left in the photic zone for NO_3^--assimilating organisms, otherwise N_2-fixation would have prevailed and $\delta^{15}N_{bulk}$ values would reflect this process (Hood et al., 2004). Assuming a fractionation in denitrification of 15‰ to 25‰ (Sigman et al., 2009; Kritee et al., 2012; Devol, 2015), we estimate around 30–45% reduction of NO_3^- at the studied location. This fraction would be higher if the isotopically heavy biomass of NO_3^- assimilators was mixed with isotopically light biomass of N_2-fixers.

To summarize, when compared to previously published results, our data show that $\delta^{15}N_{bulk}$ values were not uniform throughout the Yangtze basin during the early Ediacaran, with significantly higher $\delta^{15}N_{bulk}$ values occurring on the slope as compared to the more restricted sites at Yangtze Gorges and Lantian. We attribute these high values to a higher degree of denitrification in those settings where the surface NO_3^- reservoir would have been partially reduced through reaction with upwelling anoxic deep waters (Fig. 9). This inference is consistent with an overall redox-stratified scenario as supported by published iron-speciation data (e.g., Bowyer et al., 2017) and redox-sensitive trace metal abundances (e.g., Sahoo et al., 2016) from the Yangtze Block and provides a more detailed picture of spatial variation in the depth of the redoxcline across the Yangtze Block. This interpretation does not preclude the possibility of multiple short-lived oxygenation events in the early Ediacaran (e.g., Sahoo et al., 2016; Bowyer et al., 2017; Wang et al., 2018b), as sedimentary nitrogen isotope values alone may not be sensitive to temporal variation in the depth of redoxcline when it is below the photic zone.

5.2.2. The late Ediacaran

Average $\delta^{15}N_{bulk}$ values on the Yangtze Block decrease from the early to late Ediacaran (Fig. 7b); however, the trend of heavier values in slope sections (excluding the Yuanjia section) and a decreasing shoreward gradient persist (Fig. 5, and 7). The lightest $\delta^{15}N_{bulk}$ values, around 0‰, in the intrashelf basin are best explained by biological N_2-fixation using Mo-based nitrogenase (e.g. Zerkle et al., 2008). In the late Ediacaran, water depths across the Yangtze platform were likely shallower compared to the early Ediacaran and early Cambrian, as indicated by platform-wide carbonate deposition during this time (Fig. 2B; Zhu et al., 2003; Zhu et al., 2007b; Jiang et al., 2011). In light of this local sea-level variation and a complex paleotopographic landscape (Fig. 2B), it is possible that more proximal settings became restricted from the open ocean during the late Ediacaran, such that less fixed nitrogen was available to the photic zone and N_2-fixation dominated the ecosystem—similar to what is observed in the modern Black Sea, Baltic Sea, and Cariaco Basin (Haug et al., 1998; Wasmund et al., 2001; Fulton et al., 2012).

The lateral distribution of $\delta^{15}N_{bulk}$ values on the Yangtze Block would then reflect the variance of nitrogen speciation and its availability in the photic zone. In this way, bioavailable NO_3^- appears to have been more abundant in offshore sections and decreased shoreward. Assuming that the offshore locations continued to share a strong connection with the open ocean, the nitrogen cycle there would likely have been broadly similar to that of the early Ediacaran, where the nutrient supply and

productivity were fueled by upwelling (Fig. 9). The higher $\delta^{15}N_{bulk}$ values in the deep-water sections, compared to the intrashelf basin, may reflect a decreasing influence of N_2-fixation basinward (Figs. 5, and 7a). Lower $\delta^{15}N_{bulk}$ values in the late Ediacaran present in the Yuanjia section may have resulted from N_2-fixation because of significant distance from the zone of upwelling. The decrease in average $\delta^{15}N_{bulk}$ values in slope settings from the early to late Ediacaran could reflect a decrease in the degree of denitrification in local subsurface waters resulting from a decrease in productivity and/or deepening of the redoxcline, an increase in the influence of N_2-fixation because less NO_3^- was delivered from shallower waters as the basin became more restricted and nutrient starved, or some combination of these (Fig. 9).

5.2.3. Fortunian and late Stage 2

Average $\delta^{15}N_{bulk}$ data across the Yangtze Block from the Cambrian Fortunian-late Stage 2 are lower than those from the late Ediacaran but still higher than those from the latest Stage 2-Stage 3, and overall there is large variability in $\delta^{15}N_{bulk}$ across the Yangtze Block (−4.3‰ to 8.8‰; Figs. 5, and 7a). The nitrogen cycle during this time was likely in a transitional stage between the late Ediacaran and Cambrian Stage 3 caused by locally fluctuating redox conditions. As mentioned above, however, this interval could reflect significant periods of non-deposition or erosion. For this reason, a high-resolution correlation is difficult and signals of changing nutrient dynamics could be obscured.

5.2.4. The latest Stage 2 and Stage 3

The $\delta^{15}N_{bulk}$ values across the Yangtze Block during the latest Stage 2-Stage 3 decrease to the lowest average values observed in our compilation (ranging from −7.5‰ to 6.4‰). Most sections preserve an average $\delta^{15}N_{bulk}$ value lower than 1‰ in stratigraphic proximity to the Ni–Mo–PGE horizons. Above that, $\delta^{15}N_{bulk}$ values increase in some sections (Figs. 5, and 7a).

Light $\delta^{15}N_{bulk}$ values, less than −2‰ as present in sections from the platform, slope, and basin can be explained by two mechanisms. First, ecosystems dominated by N_2-fixation using alternative nitrogenases with V or Fe can generate $\delta^{15}N_{biomass}$ values between −6‰ and −8‰ (Zhang et al., 2014). However, the Mo limitation that would have favored these pathways can probably be ruled out. Even in the Mo-depleted, Fe-rich Archean and Proterozoic oceans, there is no convincing evidence to suggest that alternative nitrogenases with V (Vnf) or Fe (Anf) ever dominated N_2-fixation (Stüeken et al., 2016). There is no *a priori* reason to expect that molybdenum availability was lower during the early Cambrian compared to Archean-Proterozoic oceans (Siebert et al., 2005; Kendall et al., 2006; Wille et al., 2007; Scott et al., 2008).

Alternatively, non-quantitative assimilation of NH_4^+ by organisms can impart large fractionations of −4‰ to −27‰ depending on the ambient NH_4^+ concentration, yielding $\delta^{15}N_{biomass}$ values below −2‰ (Pennock et al., 1996). This scenario has been invoked to explain low $\delta^{15}N_{bulk}$ values associated with Cretaceous oceanic anoxic events and in the late Paleoproterozoic (Papineau et al., 2009; Higgins et al., 2012), and it is a reasonable interpretation for the data in this part of the succession (Fig. 9). Light $\delta^{15}N_{bulk}$ values would have been preserved where incomplete assimilation of NH_4^+ occurred in the photic zone, and a complementary ^{15}N enriched reservoir may have been captured elsewhere (Stüeken et al., 2016). Previous studies have noted that light $\delta^{15}N_{bulk}$ values are widespread on the Yangtze Block during the early Cambrian and suggested that these low values may indicate a shallow redoxcline accompanied by photic zone anoxia, possibly due to strong influx of NH_4^+-rich anoxic waters from below followed by incomplete NH_4^+ utilization by phytoplankton (Cremonese et al., 2013a; Cremonese et al., 2013b; Wang et al., 2015; Wei et al., 2017; Wang et al., 2018a). Our preferred interpretation is consistent with overwhelmingly anoxic deep waters as evidenced by other geochemical proxies such as iron-speciation (e.g., Li et al., 2017) and redox-sensitive trace element data for late Cambrian Stage 2 (e.g., Xiang et al., 2017). Considering that the most negative $\delta^{15}N_{bulk}$ value observed in our compilation is −7.5‰, the NH_4^+ concentrations in deep waters were probably equal to or lower than modern NO_3^- concentrations (~30 μM), as non-quantitative assimilation of NH_4^+ under conditions of NH_4^+ >20 μM can lead to much larger fractionations (Hoch et al., 1992). Such non-quantitative assimilation could also reflect a limitation by other nutrients in the photic zone (Moore et al., 2013), leading to incomplete utilization of NH_4^+.

Excess NH_4^+ is further supported by the TN versus TOC relationships for this interval (Fig. 6a). As mentioned in Section 5.1, linear regression yields a positive intercept on the TN-axis for the early Cambrian Jiumenchong Formation and its stratigraphic equivalents across the Yangtze Block, indicating excess, silicate-bound nitrogen. This silicate-bound nitrogen is unlikely to have been sourced from terrestrial runoff, because the Jiumenchong Formation and its stratigraphic equivalents have higher TOC than the other two formations in the studied core, for which a prominent positive intercept is not present. It is also unlikely that the nitrogen excess was controlled by lithology, as aluminum contents in the late Stage 2-Stage 3 interval in sections from an intrashelf basin (Jiulongwan section; Ling et al., 2013), the upper slope (Daotuo section; Zhai et al., 2016), and the slope (Wuhe section; Sahoo et al., 2016) are similar to those in the early Ediacaran, but clay contents in the late Stage 2-Stage 3 are actually lower (Zhai et al., 2018). Further, a cross-plot of TN versus TOC of different lithologies for the

Jiumenchong Formation in the studied core (Fig. 8) contain this positive N-intercept even in samples with higher carbonate content. The consistent appearance of the positive N-intercept for shales deposited during latest Stage 2-Stage 3 across the Yangtze Block, with a maximum in the lower slope (e.g., Kikumoto et al., 2014, and references therein), and the absence of the positive N-intercept from Ediacaran shales (Ader et al., 2014; Kikumoto et al., 2014) argues against significant control by the relative abundance of clay minerals in these samples.

Concentrations of NH_4^+ can be high when large proportions of organic matter are remineralized through microbial sulfate reduction and/or methanogenesis, as organic carbon is converted to CO_2 or CH_4, and organic nitrogen is converted to NH_4^+. Under most circumstances, sulfate is not a strong enough oxidant to oxidize NH_4^+, such that it can accumulate in localized euxinic settings and anoxic pore waters (Stüeken et al., 2016). Through this mechanism, NH_4^+ can reach high concentrations—particularly in restricted, density-stratified environments where NH_4^+ is not transported efficiently upward to the photic zone where it can be reutilized. The modern Black Sea is such a setting, with NH_4^+ concentration of ~100 μM at depth (Murray et al., 2005; Fulton et al., 2012). Additional NH_4^+ can be produced via DNRA coupled to Fe^{2+} or organic matter oxidation (Kartal et al., 2007; Lam et al., 2009; Michiels et al., 2017), although the importance of this process remains largely unexplored. In modern water masses like the Black Sea and the Benguela upwelling system, ammonium is mostly sourced from the remineralization of organic matter rather than DNRA (Kuypers et al., 2005; Murray et al., 2005). The ammonium in the water column or sediments could then be captured by illite and montmorillonite (Fig. 1; Boatman and Murray, 1982). Consistent with this scenario, data from the Black Sea contain a significant positive N-intercept when plotted versus TOC (570 ppm; Fulton et al., 2012), while data from open marine sediments exhibit much smaller N-intercepts (40−50 ppm; Muzuka and Hillaire-Marcel, 1999; Li and Bebout, 2005).

Total organic carbon values in our studied core are generally high when $\delta^{15}N_{bulk}$ values are negative. This suggests a high flux of export production and commensurately high deep-water respiratory demand. This could have also resulted in widespread water-column sulfate reduction, as suggested by high Fe_P/Fe_{HR} ratios indicating the development of euxinia on the outer shelf and slope of Yangtze Block during this time (e.g. Canfield et al., 2008; Feng et al., 2014). The resulting excess NH_4^+ in the anoxic water column and sediment pore waters could then be adsorbed by clay minerals, leading to the observed positive N-intercepts. Overall, this scenario of excess NH_4^+ further supports the proposition of non-quantitative NH_4^+ assimilation by organisms in stratigraphic proximity to the negative $\delta^{15}N_{bulk}$ horizons, and is also consistent with the majority

of previously published interpretations of the redox state of basinal waters at this time.

5.3. Implications for life

The distribution of $\delta^{15}N_{bulk}$ values on the Yangtze Block across the Ediacaran-Cambrian transition implies broadly that the supply of fixed nitrogen may have been higher, at least in this basin, than is suggested by earlier Mesoproterozoic records (Stüeken, 2013; Koehler et al., 2016). Restriction of positive $\delta^{15}N_{bulk}$ to shallow facies in the Mesoproterozoic Belt Supergroup (~1.4 Ga; Stüeken, 2013), Bangemall Supergroup (~1.5 Ga; Stüeken, 2013), and Roper Group (~1.4−1.5 Ga; Koehler et al., 2016) indicates a largely anaerobic nitrogen cycle in offshore environments and an aerobic nitrogen cycle with NO_3^- restricted to the photic zone in nearshore settings. This was not the case during the Ediacaran and early Cambrian in the Yangtze Block. A significant aerobic nitrogen cycle appears to have been present in the Ediacaran of South China, with abundant NO_3^- available in surface waters. Abundant nitrate could have contributed to the evolution of macroscopic multicellular algae in the Ediacaran (Zhu et al., 2007a; Zhu, 2010). Although data from one basin cannot capture global trends in marine nitrogen cycling, it is conceivable that they may in part reflect global biogeochemical trends—eukaryotic algae rising to ecological prominence in the Cryogenian, evidenced by molecular fossil records (Brocks et al., 2017), could have significantly changed the architecture of the biological pump, allowing for more fixed nitrogen to accumulate in deeper waters.

Additionally, our analysis provides supporting evidence for a temporal change in the position of the redoxcline on the Yangtze Block during the Proterozoic-Phanerozoic transition. High $\delta^{15}N_{bulk}$ values combined with other redox proxies in the Ediacaran (e.g., Bowyer et al., 2017) probably reflect a relatively deep chemocline (likely near the base of the photic zone) with some spatial heterogeneity. This deeper redoxcline could have provided niches in shallow marine environments for metazoans with relatively high metabolic oxygen demands, consistent with the presence of some Ediacaran metazoan fauna on the Yangtze Block (e.g. Zhu et al., 2007a; Zhu et al., 2008; Zhu, 2010; Jiang et al., 2011). In the latest Cambrian Stage 2, an overall shallower redoxcline (probably within photic zone) suggested by low $\delta^{15}N_{bulk}$ values, is consistent with scenarios that have been proposed for extinctions of small shelly fossils (Zhu et al., 2007a; Zhu, 2010; Wang et al., 2018a). Such a shallow chemocline in the early Cambrian could have been linked to higher primary and export production, consistent with high observed TOC values (Fig. 3).

6. Conclusions

Our geochemical study of early Ediacaran to early Cambrian strata preserved in a drill core taken from the slope of the Yangtze Block, combined with previously reported $\delta^{15}N_{bulk}$ data from other sections at different paleo-water depths, confirm that average $\delta^{15}N_{bulk}$ values decreased from the early Ediacaran to early Cambrian across the Yangtze Block. This suggests a systematic transition in the regional nitrogen cycle across this interval. In the early Ediacaran, $\delta^{15}N_{bulk}$ values reflect a basinal gradient, with the highest values occurring in the slope section of the Upper Yangtze, and a declining trend toward more restricted profiles (Yangtze Gorges and Lantian regions), suggesting that more intense denitrification was occurring in open slope settings. These data may reflect upwelling of anoxic deep water along the slope and a shoaling of the redoxcline near our studied location. High $\delta^{15}N_{bulk}$ values on the slope decrease in the late Ediacaran, and nearshore $\delta^{15}N_{bulk}$ values from this time are near 0‰, indicating N_2-fixation dominated nearshore environments. This temporary dearth in nitrogen availability could have been caused by decreasing water depth and isolation of intra-shelf settings in the late Ediacaran. However, offshore sections show high $\delta^{15}N_{bulk}$ values at this time, implying the presence of significant fixed nitrogen (likely in the form of NO_3^-) in the photic zone. During the following Cambrian Fortunian to late Stage 2, highly variable $\delta^{15}N_{bulk}$ values indicate the nitrogen cycle was likely in a transitional state.

During the latest Stage 2-Stage 3, $\delta^{15}N_{bulk}$ values decrease to near 0‰ or lower in all settings across the Yangtze Block in stratigraphic proximity to the Ni–Mo deposits. These light values are most parsimoniously interpreted as evidence of widespread partial uptake of NH_4^+. The TN versus TOC relationships further substantiate that NH_4^+ concentrations were high throughout most of the basin at this time, potentially linked to large amounts of organic matter remineralization by sulfate reduction under euxinic conditions. The redoxcline could have been fairly shallow at the time, such that abundant NH_4^+ was delivered to surface waters.

Overall, our study suggests that nitrogen—either in the form of NO_3^- or NH_4^+—was more bioavailable during the Ediacaran and early Cambrian than during the Mesoproterozoic. In the modern ocean, environmental factors such as nutrient and oxidant availability play a first order role in dictating ecosystem structure and complexity. In turn, the availability, distribution, and temporal stability of habit space are critical factors in directing evolutionary trends. These influences should be given due consideration with respect to the Phanerozoic transition, particularly in light of substantial evidence for dynamically changing conditions.

Acknowledgements

The authors acknowledge funding support from the NSF FESD and Earth-Life Transitions programs (T.L.), the NASA Astrobiology Institute under Cooperative Agreement No. NNA15BB03A issued through the Science Mission Directorate (T.L.), the key project of the Natural Science Foundation of China (C.-F.C.) (No. 41730424), and the program of China Scholarships Council (Y.C.) (No. 201504910582). Nitrogen and carbon isotope analyses were funded by startup funds from Virginia Tech to B.C.G. We thank Dr. Chuanming Zhou, Dr. Hongfei Ling, and Dr. Maoyan Zhu for the helpful suggestions on the stratigraphic correlation on the Yangtze Block. We also thank Xiqiang Zhou, Lei Xiang, Taiyu Huang, and Lina Zhai for their helpful advice and beneficial discussions.

Appendix A. Supplementary Data

References

Ader, M., Boudou, J.-P., Javoy, M., Goffe, B. and Daniels, E. (1998) Isotope study on organic nitrogen of Westphalian anthracites from the Western Middle field of Pennsylvania (USA) and from the Bramsche Massif (Germany). *Org. Geochem.* **29**, 315-323.

Ader, M., Sansjofre, P., Halverson, G.P., Busigny, V., Trindade, R.I., Kunzmann, M. and Nogueira, A.C. (2014) Ocean redox structure across the Late Neoproterozoic Oxygenation Event: A nitrogen isotope perspective. *Earth Planet. Sci. Lett.* **396**, 1-13.

Ader, M., Thomazo, C., Sansjofre, P., Busigny, V., Papineau, D., Laffont, R., Cartigny, P. and Halverson, G.P. (2016) Interpretation of the nitrogen isotopic composition of Precambrian sedimentary rocks: Assumptions and perspectives. *Chem. Geol.* **285**, 35537-35550.

Altabet, M.A. (1988) Variations in nitrogen isotopic composition between sinking and suspended particles: implications for nitrogen cycling and particle transformation in the open ocean. *Deep Sea Res. Part A. Oceanograph. Res. Pap.* **35**, 535-554.

Altabet, M.A. and Francois, R. (1994) Sedimentary nitrogen isotopic ratio as a recorder for surface ocean nitrate utilization. *Global Biogeochem. Cycles* **8**, 103-116.

Altabet, M.A., Higginson, M.J. and Murray, D.W. (2002) The effect of millennial-scale changes in Arabian Sea denitrification on atmospheric CO_2. *Nature* **415**, 159-162.

Altabet, M.A., Pilskaln, C., Thunell, R., Pride, C., Sigman, D., Chavez, F. and Francois, R. (1999) The nitrogen isotope biogeochemistry of sinking particles from the margin of the Eastern North Pacific. *Deep Sea Res. Part I Oceanograph* **46**, 655-679.

Beaumont, V. and Robert, F. (1999) Nitrogen isotope ratios of kerogens in Precambrian cherts: a record of the evolution of atmosphere chemistry? *Precambrian Res.* **96**, 63-82.

Bebout, G.E. and Fogel, M.L. (1992) Nitrogen-isotope compositions of metasedimentary rocks in the Catalina Schist, California: implications for metamorphic devolatilization history. *Geochim. Cosmochim. Acta* **56**, 2839-2849.

Berkner, L.V. and Marshall, L.C. (1965) On the Origin and Rise of Oxygen Concentration in the Earth's Atmosphere. *Journal of the Atmospheric Sciences* **22**, 225-261.

Berner, R.A. (2006) Geological nitrogen cycle and atmospheric N_2 over Phanerozoic time. *Geology* **34**, 413-415.

Boatman, C.D. and Murray, J.W. (1982) Modeling exchangeable NH_4^+ adsorption in marine sediments: Process and controls of adsorption. *Limnol. Oceanogr.* **27**, 99-110.

Bowring, S.A., Grotzinger, J.P., Condon, D.J., Ramezani, J., Newall, M.J. and Allen, P.A. (2007) Geochronologic constraints on the chronostratigraphic framework of the Neoproterozoic Huqf Supergroup, Sultanate of Oman. *Am. J. Sci.* **32**, S93-S94.

Bowyer, F., Wood, R.A. and Poulton, S.W. (2017) Controls on the evolution of Ediacaran metazoan ecosystems: A redox perspective. *Geobiology* **15**, 516-551.

Boyd, S.R. and Philippot, P. (1998) Precambrian Amonium Biogeochemistry: a study of the Moine metasediments, Scotland. *Chem. Geol.* **144**, 257-268.

Brandes, J.A. and Devol, A.H. (2002) A global marine - fixed nitrogen isotopic budget: Implications for Holocene nitrogen cycling. *Global Biogeochem. Cycles* **16**, 67-61-67-14.

Brandes, J.A., Devol, A.H., Yoshinari, T., Jayakumar, D.A. and Naqvi, S.W.A. (1998) Isotopic composition of nitrate in the central Arabian Sea and eastern tropical North Pacific: A tracer for mixing and nitrogen cycles. *Limnol. Oceanogr.* **43**, 1680-1689.

Brasier, M.D. (1979) The Cambrian radiation event, In *The Origin of Major Invertebrate Groups*, (eds. House, M.R.). Systematics Association Special Volume. pp. 103-159.

Brasier, M.D. (1992) Paleoceanography and Changes in the Biological Cycling of Phosphorus across the Precambrian—Cambrian Boundary, In *Origin and Early Evolution of the Metazoa*, (eds. Lipps, J.H., Signor, P.W.). Springer, Boston, MA. pp. 483-523.

Bristow, T.F., Kennedy, M.J., Derkowski, A., Droser, M.L., Jiang, G. and Creaser, R.A. (2009) Mineralogical constraints on the paleoenvironments of the Ediacaran Doushantuo Formation. *Proc. Natl. Acad. Sci.* **106**, 13190-13195.

Brocks, J.J., Jarrett, A.J.M., Sirantoine, E., Hallmann, C., Hoshino, Y. and Liyanage, T. (2017) The rise of algae in Cryogenian oceans and the emergence of animals. *Nature* **548**, 578-581.

Brunner, B., Contreras, S., Lehmann, M.F., Matantseva, O., Rollog, M., Kalvelage, T., Klockgether, G., Lavik, G., Jetten, M.S. and Kartal, B. (2013) Nitrogen isotope effects induced by anammox bacteria. *Proc. Natl. Acad. Sci.* **110**, 18994-18999.

Cai, C., Xiang, L., Yuan, Y., He, X., Chu, X., Chen, Y. and Xu, C. (2015) Marine C, S and N biogeochemical processes in the redox-stratified early Cambrian Yangtze ocean. *Journal of the Geological Society* **172**, 390-406.

Calvert, S.E. (2004) Beware intercepts: interpreting compositional ratios in multi-component sediments and sedimentary rocks. *Org. Geochem.* **35**, 981-987.

Campbell, I.H. and Allen, C.M. (2008) Formation of supercontinents linked to increases in atmospheric oxygen. *Nat. Geosci.* **1**, 554-558.

Canfield, D.E. (2005) The early history of atmospheric oxygen: homage to Robert A. Garrels. *Annu. Rev. Earth Planet. Sci.* **33**, 1-36.

Canfield, D.E., Glazer, A.N. and Falkowski, P.G. (2010) The evolution and future of Earth's nitrogen cycle. *Science* **330**, 192-196.

Canfield, D.E., Poulton, S.W., Knoll, A.H., Narbonne, G.M., Ross, G., Goldberg, T. and Strauss, H. (2008) Ferruginous conditions dominated later neoproterozoic deep-water chemistry. *Science* **321**, 949.

Canfield, D.E., Poulton, S.W. and Narbonne, G.M. (2007) Late-Neoproterozoic deep-ocean oxygenation and the rise of animal life. *Science* **315**, 92-95.

Casciotti, K.L. (2009) Inverse kinetic isotope fractionation during bacterial nitrite oxidation. *Geochim. Cosmochim. Acta* **73**, 2061-2076.

Casciotti, K.L., Sigman, D.M. and Ward, B.B. (2003) Linking Diversity and Stable Isotope Fractionation in Ammonia-Oxidizing Bacteria. *Geomicrobiology Journal* **20**, 335-353.

Catling, D.C., Glein, C.R., Zahnle, K.J. and Mckay, C.P. (2005) Why O_2 is required by complex life on habitable planets and the concept of planetary "oxygenation time". *Astrobiology* **5**, 415.

Charvet, J. (2013) The Neoproterozoic–Early Paleozoic tectonic evolution of the South China Block: An overview. *Journal of Asian Earth Sciences* **74**, 198-209.

Chen, D., Wang, J., Qing, H., Yan, D. and Li, R. (2009) Hydrothermal venting activities in the Early Cambrian, South China: Petrological, geochronological and stable isotopic constraints. *Chem. Geol.* **258**, 168-181.

Chen, D., Zhou, X., Fu, Y., Wang, J. and Yan, D. (2015a) New U–Pb zircon ages of the Ediacaran–Cambrian boundary strata in South China. *Terra Nova* **27**, 62-68.

Chen, P. (1984) Discovery of lower Cambrian small shelly fossils from Jijiapo, Yichang, west Hubei and its significance. *Professional Papers of Stratigraphy & Palaeontology*, 49-66.

Chen, X., Ling, H.F., Vance, D., Shieldszhou, G.A., Zhu, M., Poulton, S.W., Och, L.M., Jiang, S.Y., Li, D. and Cremonese, L. (2015b) Rise to modern levels of ocean oxygenation coincided with the Cambrian radiation of animals. *Nat. Commun.* **6**, 7142.

Compston, W., Zhang, Z., Cooper, J.A., Ma, G. and Jenkins, R.J.F. (2008) Further SHRIMP geochronology on the early Cambrian of South China. *Am. J. Sci.* **308**, 399-420.

Condon, D., Zhu, M., Bowring, S., Wang, W., Yang, A. and Jin, Y. (2005) U-Pb Ages from the Neoproterozoic Doushantuo Formation, China. *Science* **308**, 95-98.

Cremonese, L., Shields-Zhou, G., Struck, U., Ling, H.-F., Och, L., Chen, X. and Li, D. (2013a) Marine biogeochemical cycling during the early Cambrian constrained by a nitrogen and organic carbon isotope study of the Xiaotan section, South China. *Precambrian Res.* **225**, 148-165.

Cremonese, L., Shields-Zhou, G.A., Struck, U., Ling, H.-F. and Och, L.M. (2013b) Nitrogen and organic carbon isotope stratigraphy of the Yangtze Platform during the Ediacaran–Cambrian transition in South China. *Palaeogeogr. Palaeoclimatol. Palaeoecol.* **398**, 165-186.

Dahl, T.W., Connelly, J.N., Kouchinsky, A., Gill, B.C., Månsson, S.F. and Bizzarro, M. (2017) Reorganisation of Earth's biogeochemical cycles briefly oxygenated the oceans 520 Myr ago. *Geochemical Perspectives Letters* **3**, 210-220.

Dahl, T.W., Hammarlund, E.U., Anbar, A.D., Bond, D.P., Gill, B.C., Gordon, G.W., Knoll, A.H., Nielsen, A.T., Schovsbo, N.H. and Canfield, D.E. (2010) Devonian rise in atmospheric oxygen correlated to the radiations of terrestrial plants and large predatory fish. *Proc. Natl. Acad. Sci.* **107**, 17911-17915.

Dalsgaard, T., Bo, T., Farías, L. and Revsbech, N.P. (2012) Anammox and denitrification in the oxygen minimum zone of the eastern South Pacific. *Limnol. Oceanogr.* **57**, 1331-1346.

Devol, A.H. (2015) Denitrification, Anammox, and N_2 production in marine sediment. *Annu. Rev. Marine Sci.* **7**, 403-423.

Falkowski, P.G. (1997) Evolution of the nitrogen cycle and its influence on the biological sequestration of CO_2 in the ocean. *Nature* **387**, 272-275.

Feng, L., Li, C., Huang, J., Chang, H. and Chu, X. (2014) A sulfate control on marine mid-depth euxinia on the early Cambrian (ca. 529–521 Ma) Yangtze platform, South China. *Precambrian Res.* **246**, 123-133.

Fike, D., Grotzinger, J., Pratt, L. and Summons, R. (2006) Oxidation of the Ediacaran ocean. *Nature* **444**, 744-747.

Finnegan, S., Heim, N.A., Peters, S.E. and Fischer, W.W. (2012) Climate change and the selective signature of the Late Ordovician mass extinction. *Proceedings of the National Academy of Sciences*.

Freudenthal, T., Wagner, T., Wenzhöfer, F., Zabel, M. and Wefer, G. (2001) Early diagenesis of organic matter from sediments of the eastern subtropical Atlantic: Evidence from stable nitrogen and carbon isotopes. *Geochim. Cosmochim. Acta* **65**, 1795-1808.

Fuchsman, C.A., Murray, J.W. and Konovalov, S.K. (2008) Concentration and natural stable isotope profiles of nitrogen species in theBlack Sea. *Marine Chem.* **111**, 90-105.

Fulton, J.M., Arthur, M.A. and Freeman, K.H. (2012) Black Sea nitrogen cycling and the preservation of phytoplankton $\delta^{15}N$ signals during the Holocene. *Global Biogeochem. Cycles* **26**, GB2030-GB2044.

Fussel, J., Lam, P., Lavik, G., Jensen, M.M., Holtappels, M., Gunter, M. and Kuypers, M.M.M. (2012) Nitrite oxidation in the Namibian oxygen minimum zone. *ISME J.* **6**, 1200-1209.

Gaye-Haake, B., Lahajnar, N., Emeis, K.-C., Unger, D., Rixen, T., Suthhof, A., Ramaswamy, V., Schulz, H., Paropkari, A. and Guptha, M. (2005) Stable nitrogen isotopic ratios of sinking particles and sediments from the northern Indian Ocean. *Marine Chem.* **96**, 243-255.

Goldberg, T., Strauss, H., Guo, Q. and Liu, C. (2007) Reconstructing marine redox conditions for the Early Cambrian Yangtze Platform: evidence from biogenic sulphur and organic carbon isotopes. *Palaeogeogr. Palaeoclimatol. Palaeoecol.* **254**, 175-193.

Gradstein, F.M., Ogg, J.G., Schmitz, M.D. and Ogg, G.M. (2012) *The Geologic Time Scale 2012*. Elsevier.

Granger, J., Prokopenko, M.G., Sigman, D.M., Mordy, C.W., Morse, Z.M., Morales, L.V., Sambrotto, R.N. and Plessen, B. (2011) Coupled nitrification - denitrification in sediment of the eastern Bering Sea shelf leads to ^{15}N enrichment of fixed N in shelf waters. *J. Geophys. Res.* **116**, C11006.

Guo, J., Li, Y. and Li, G. (2014) Small shelly fossils from the early Cambrian Yanjiahe Formation, Yichang, Hubei, China. *Gondwana Res.* **25**, 999-1007.

Guo, Q., Deng, Y., Hippler, D., Franz, G. and Zhang, J. (2016) REE and trace element patterns from organic-rich rocks of the Ediacaran–Cambrian transitional interval. *Gondwana Res.* **36**, 94-106.

Guo, Q., Strauss, H., Liu, C., Goldberg, T., Zhu, M., Pi, D., Heubeck, C., Vernhet, E., Yang, X. and Fu, P. (2007) Carbon isotopic evolution of the terminal Neoproterozoic and early Cambrian: Evidence from the Yangtze Platform, South China. *Palaeogeogr. Palaeoclimatol. Palaeoecol.* **254**, 140-157.

Guo, Q., Strauss, H., Zhu, M., Zhang, J., Yang, X., Lu, M. and Zhao, F. (2013) High resolution organic carbon isotope stratigraphy from a slope to basinal setting on the Yangtze Platform, South China: Implications for the Ediacaran–Cambrian transition. *Precambrian Res.* **225**, 209-217.

Halverson, G.P., Dudás, F.Ö., Maloof, A.C. and Bowring, S.A. (2007) Evolution of the $^{87}Sr/^{86}Sr$ composition of Neoproterozoic seawater. *Palaeogeogr. Palaeoclimatol. Palaeoecol.* **256**, 103-129.

Halverson, G.P., Hoffman, P.F., Schrag, D.P., Maloof, A.C. and Rice, A.H.N. (2005) Toward a Neoproterozoic composite carbon-isotope record. *Geol. Soc. Am. Bull.* **117**, 1181-1207.

Hammarlund, E.U., Gaines, R.R., Prokopenko, M.G., Qi, C., Hou, X.-G. and Canfield, D.E. (2017) Early Cambrian oxygen minimum zone-like conditions at Chengjiang. *Earth Planet. Sci. Lett.* **475**, 160-168.

Han, S., Zhang, J., Li, Y., Horsfield, B., Tang, X., Jiang, W. and Chen, Q. (2013) Evaluation of Lower Cambrian Shale in Northern Guizhou Province, South China: Implications for Shale Gas Potential. *Energy & Fuels* **27**, 2933-2941.

Haug, G.H., Pedersen, T.F., Sigman, D.M., Calvert, S.E., Nielsen, B. and Peterson, L.C. (1998) Glacial/interglacial variations in production and nitrogen fixation in the Cariaco Basin during the last 580 kyr. *Paleoceanography* **13**, 427–432.

Hayes, J.M., Wedeking, K.W. and Kaplan, I.R. (1983) Precambrian organic geochemistry - Preservation of the record, in: Schopf, J.W. (Ed.), Earth's Earliest Biosphere, Its Origin and Evolution. Princeton University Press, Princeton, NJ, pp. 93–134.

Higgins, M.B., Robinson, R.S., Husson, J.M., Carter, S.J. and Pearson, A. (2012) Dominant eukaryotic export production during ocean anoxic events reflects the importance of recycled NH_4^+. *Proc. Natl. Acad. Sci.* **109**, 2269-2274.

Ho, T.Y., Taylor, G.T., Astor, Y., Varela, R., Müller-Karger, F. and Scranton, M.I. (2004) Vertical and temporal variability of redox zonation in the water column of the Cariaco Basin: implications for organic carbon oxidation pathways. *Marine Chem.* **86**, 89-104.

Hoch, M.P., Fogel, M.L. and Kirchman, D.L. (1992) Isotope Fractionation Associated with Ammonium Uptake by a Marine Bacterium. *Limnol. Oceanogr.* **37**, 1447-1459.

Hoffman, P.F., Abbot, D.S., Ashkenazy, Y., Benn, D.I., Brocks, J.J., Cohen, P.A., Cox, G.M., Creveling, J.R., Donnadieu, Y. and Erwin, D.H. (2017) Snowball Earth climate dynamics and Cryogenian geology-geobiology. *Sci. Adv.* **3**, e1600983.

Holland, H.D. (2006) The oxygenation of the atmosphere and oceans. *Proceedings of the Royal Society B: Biological Sciences* **361**, 903-915.

Hood, R.R., Coles, V.J. and Capone, D.G. (2004) Modeling the distribution of Trichodesmium and nitrogen fixation in the Atlantic Ocean. *J. Geophys. Res.: Oceans* **109**, C06006.

Jia, Y. (2006) Nitrogen isotope fractionations during progressive metamorphism: A case study from the Paleozoic Cooma metasedimentary complex, southeastern Australia. *Geochim. Cosmochim. Acta* **70**, 5201-5214.

Jiang, G., Shi, X., Zhang, S., Wang, Y. and Xiao, S. (2011) Stratigraphy and paleogeography of the Ediacaran Doushantuo Formation (ca. 635–551Ma) in South China. *Gondwana Res.* **19**, 831-849.

Jiang, G., Sohl, L.E. and Christieblick, N. (2003) Neoproterozoic stratigraphic comparison of the Lesser Himalaya (India) and Yangtze block (South China): Paleogeographic implications. *Geology* **31**, 917-920.

Jiang, G., Wang, X., Shi, X., Xiao, S., Zhang, S. and Dong, J. (2012) The origin of decoupled carbonate and organic carbon isotope signatures in the early Cambrian (ca. 542–520Ma) Yangtze platform. *Earth Planet. Sci. Lett.* **317**, 96-110.

Jiang, S.Y., Pi, D.H., Heubeck, C., Frimmel, H., Liu, Y.P., Deng, H.L., Ling, H.F. and Yang, J.H. (2009) Early Cambrian ocean anoxia in South China. *Nature* **459**, E5-6; discussion E6.

Jin, C., Li, C., Algeo, T.J., Planavsky, N.J., Cui, H., Yang, X., Zhao, Y., Zhang, X. and Xie, S. (2016) A highly redox-heterogeneous ocean in South China during the early Cambrian (~529–514Ma): Implications for biota-environment co-evolution. *Earth Planet. Sci. Lett.* **441**, 38-51.

Johnston, D.T., Poulton, S.W., Goldberg, T., Sergeev, V.N., Podkovyrov, V., Vorob'Eva, N.G., Bekker, A. and Knoll, A.H. (2012) Late Ediacaran redox stability and metazoan evolution. *Earth Planet. Sci. Lett.* **s335–336**, 25-35.

Karl, D., Michaels, A., Bergman, B., Capone, D., Carpenter, E., Letelier, R., Lipschultz, F., Paerl, H., Sigman, D. and Stal, L. (2002) Dinitrogen fixation in the world's oceans. *Biogeochemistry* **57/58**, 47-98.

Kartal, B., Kuypers, M.M.M., Lavik, G., †, J.S., Camp, H.J.M.O.D., Jetten, M.S.M. and Strous, M. (2007) Anammox bacteria disguised as denitrifiers: nitrate reduction to dinitrogen gas via nitrite and ammonium. *Environ. Microbiol* **9**, 635.

Kendall, B., Anbar, A.D., Gordon, G., Arnold, G.L. and Creaser, R.A. (2006) Constraining the redox state of the Proterozoic deep oceans using the Mo isotope systematics of euxinic black shales, Geological Society of America Abstracts with Programs.

Kendall, B., Creaser, R.A., Reinhard, C.T., Lyons, T.W. and Anbar, A.D. (2015a) Transient episodes of mild environmental oxygenation and oxidative continental weathering during the late Archean. *Sci. Adv.* **1**, e1500777-e1500777.

Kendall, B., Komiya, T., Lyons, T.W., Bates, S.M., Gordon, G.W., Romaniello, S.J., Jiang, G., Creaser, R.A., Xiao, S. and Mcfadden, K. (2015b) Uranium and molybdenum isotope evidence for an episode of widespread ocean oxygenation during the late Ediacaran Period. *Geochim. Cosmochim. Acta* **156**, 173-193.

Kenrick, P. and Crane, P.R. (1997) The origin and early evolution of plants on land. *Nature* **389**, 33-39.

Kikumoto, R., Tahata, M., Nishizawa, M., Sawaki, Y., Maruyama, S., Shu, D., Han, J., Komiya, T., Takai, K. and Ueno, Y. (2014) Nitrogen isotope chemostratigraphy of the Ediacaran and Early Cambrian platform sequence at Three Gorges, South China. *Gondwana Res.* **25**, 1057-1069.

Knoll, A.H. (2017) Biogeochemistry: Food for early animal evolution. *Nature* **548**, 528-530.

Knoll, A.H. and Follows, M.J. (2016) A bottom-up perspective on ecosystem change in Mesozoic oceans. *Proceedings of the Royal Society B: Biological Sciences* **283**, 20161755.

Koehler, M.C., Stüeken, E.E., Kipp, M.A., Buick, R. and Knoll, A.H. (2016) Spatial and temporal trends in Precambrian nitrogen cycling: a Mesoproterozoic offshore nitrate minimum. *Geochim. Cosmochim. Acta* **198**, 315-337.

Kritee, K., Sigman, D.M., Granger, J., Ward, B.B., Jayakumar, A. and Deutsch, C. (2012) Reduced isotope fractionation by denitrification under conditions relevant to the ocean. *Geochim. Cosmochim. Acta* **92**, 243-259.

Kuypers, M.M.M., G, L., D, W., M, S., BM, F., R, A., BB, J. and MS, J. (2005) Massive nitrogen loss from the Benguela upwelling system through anaerobic ammonium oxidation. *Proc. Natl. Acad. Sci.* **102**, 6478.

Kuypers, M.M.M., Sliekers, A.O., Lavik, G., Schmid, M., Jørgensen, B.B., Kuenen, J.G., Sinninghe Damsté, J.S., Strous, M. and Jetten, M.S. (2003) Anaerobic ammonium oxidation by anammox bacteria in the Black Sea. *Nature* **422**, 608.

Kuypers, M.M.M., van Breugel, Y., Schouten, S., Erba, E. and Damsté, J.S.S. (2004) N_2-fixing cyanobacteria supplied nutrient N for Cretaceous oceanic anoxic events. *Geology* **32**, 853-856.

Lam, P., Lavik, G., Jensen, M.M., van de Vossenberg, J., Schmid, M., Woebken, D., Gutiérrez, D., Amann, R., Jetten, M.S. and Kuypers, M.M. (2009) Revising the nitrogen cycle in the Peruvian oxygen minimum zone. *Proc. Natl. Acad. Sci.* **106**, 4752-4757.

Landing, E., Bowring, S.A., Davidek, K.L., Westrop, S.R., Geyer, G. and Heldmaier, W. (1998) Duration of the Early Cambrian: U-Pb ages of volcanic ashes from Avalon and Gondwana. *Canadian Journal of Earth Sciences* **35**, 329-338.

Lehmann, M.F., Bernasconi, S.M., Barbieri, A. and McKenzie, J.A. (2002) Preservation of organic matter and alteration of its carbon and nitrogen isotope composition during simulated and in situ early sedimentary diagenesis. *Geochim. Cosmochim. Acta* **66**, 3573-3584.

Lenton, T.M., Dahl, T.W., Daines, S.J., Mills, B.J., Ozaki, K., Saltzman, M.R. and Porada, P. (2016) Earliest land plants created modern levels of atmospheric oxygen. *Proc. Natl. Acad. Sci.* **113**, 9704.

Li, C., Jin, C., Planavsky, N.J., Algeo, T.J., Cheng, M., Yang, X., Zhao, Y. and Xie, S. (2017) Coupled oceanic oxygenation and metazoan diversification during the early–middle Cambrian? *Geology* **45**, 743-746.

Li, C., Love, G.D., Lyons, T.W., Fike, D.A., Sessions, A.L. and Chu, X. (2010) A stratified redox model for the Ediacaran ocean. *Science* **328**, 80-83.

Li, G.X., Shuhai (2004) Tannuolina and Micrina (Tannuolinidae) from the Lower Cambrian of Eastern Yunnan, South China, and Their Scleritome Reconstruction. *J. Paleontol.* **78**, 900-913.

Li, L. and Bebout, G.E. (2005) Carbon and nitrogen geochemistry of sediments in the Central American convergent margin: Insights regarding subduction input fluxes, diagenesis, and paleoproductivity. *Journal of Geophysical Research: Solid Earth* **110**, B11202.

Li, M.-C., Ding, H., Jiao, K. and Yao, S.-P. (2012) Organic petrology of Niutitang Formation in Shancha, western Hunan Province. *China. Nat. Geosci* **23**, 1077-1089 (in Chinese with English abstract).

Li, M., Chen, J., Wang, T., Zhong, N. and Shi, S. (2018) Nitrogen isotope and trace element composition characteristics of the Lower Cambrian Niutitang Formation shale in the upper -middle Yangtze region, South China. *Palaeogeogr. Palaeoclimatol. Palaeoecol.* **501**, 1-12.

Li, Z.X., Bogdanova, S.V., Collins, A.S., Davidson, A., Waele, B.D., Ernst, R.E., Fitzsimons, I.C.W., Fuck, R.A., Gladkochub, D.P. and Jacobs, J. (2008) Assembly, configuration, and break-up history of Rodinia: A synthesis. *Precambrian Res.* **160**, 179-210.

Lindell, D. and Post, A.F. (1995) Ultraphytoplankton succession is triggered by deep winter mixing in the Gulf of Aqaba (Eilat), Red Sea. *Limnol. Oceanogr.* **40**, 1130-1141.

Ling, H.F., Chen, X., Li, D., Wang, D., Shields-Zhou, G.A. and Zhu, M. (2013) Cerium anomaly variations in Ediacaran–earliest Cambrian carbonates from the Yangtze Gorges area, South China: Implications for oxygenation of coeval shallow seawater. *Precambrian Res.* **225**, 110-127.

Lipschultz, F., Wofsy, S.C., Ward, B.B., Codispoti, L.A., Friedrich, G. and Elkins, J.W. (1990) Bacterial transformations of inorganic nitrogen in the oxygen-deficient waters of the Eastern Tropical South Pacific Ocean. *Deep Sea Res. Part A. Oceanograph. Res. Pap.* **37**, 1513-1541.

Liu, P., Yin, C., Chen, S., Tang, F. and Gao, L. (2013) The biostratigraphic succession of acanthomorphic acritarchs of the Ediacaran Doushantuo Formation in the Yangtze Gorges area, South China and its biostratigraphic correlation with Australia. *Precambrian Res.* **225**, 29-43.

Maloof, A.C., Porter, S.M., Moore, J.L., Dudás, F.Ö., Bowring, S.A., Higgins, J.A., Fike, D.A. and Eddy, M.P. (2010) The earliest Cambrian record of animals and ocean geochemical change. *Geological Society of America Bulletin* **122**, 1731-1774.

Mather, T.A., Pyle, D.M. and Allen, A.G. (2004) Volcanic source for fixed nitrogen in the early Earth's atmosphere. *Geology* **32**, 905-908.

McCready, R.G.L., Gould, W.D. and Barendregt, R.W. (1983) Nitrogen isotope fractionation during the reduction of NO_3^- to

NH_4^+ by Desulfovibrio sp. *Can. J. Microbiology* **29**, 231-234.

Mcfadden, K.A., Huang, J., Chu, X., Jiang, G., Kaufman, A.J., Zhou, C., Yuan, X. and Xiao, S. (2008) Pulsed oxidation and biological evolution in the Ediacaran Doushantuo Formation. *Proc. Natl. Acad. Sci.* **105**, 3197-3202.

Michiels, C.C., Darchambeau, F., Roland, F.A.E., Morana, C., Lliros, M., Garcia-Armisen, T., Thamdrup, B., Borges, A.V., Canfield, D.E., Servais, P., Descy, J.-P. and Crowe, S.A. (2017) Iron-dependent nitrogen cycling in a ferruginous lake and the nutrient status of Proterozoic oceans. *Nat. Geosci.* **10**, 217-221.

Mingram, B. and Bräuer, K. (2001) Ammonium concentration and nitrogen isotope composition in metasedimentary rocks from different tectonometamorphic units of the European Variscan Belt. *Geochim. Cosmochim. Acta* **65**, 273-287.

Moore, C., Mills, M., Arrigo, K., Berman-Frank, I., Bopp, L., Boyd, P., Galbraith, E., Geider, R.J., Guieu, C. and Jaccard, S. (2013) Processes and patterns of oceanic nutrient limitation. *Nat. Geosci.* **6**, 701-710.

Morales, L.V., Granger, J., Chang, B.X., Prokopenko, M.G., Plessen, B., Gradinger, R. and Sigman, D.M. (2014) Elevated $^{15}N/^{14}N$ in particulate organic matter, zooplankton, and diatom frustule-bound nitrogen in the ice-covered water column of the Bering Sea eastern shelf. *Deep Sea Res. Part II Topical Studies in Oceanography* **109**, 100-111.

Murray, J.W., Fuchsman, C., Kirkpatrick, J., Paul, B. and Konovalov, S.K. (2005) Species and $\delta^{15}N$ Signatures of nitrogen Transformations in the Suboxic Zone of the Black Sea. *Oceanography* **18**, 36-47.

Muzuka, A.N.N. and Hillaire-Marcel, C. (1999) Burial rates of organic matter along the eastern Canadian margin and stable isotope constraints on its origin and diagenetic evolution. *Marine Geology* **160**, 251-270.

Nishizawa, M., Miyazaki, J., Makabe, A., Koba, K. and Takai, K. (2014) Physiological and isotopic characteristics of nitrogen fixation by hyperthermophilic methanogens: Key insights into nitrogen anabolism of the microbial communities in Archean hydrothermal systems. *Geochim. Cosmochim. Acta* **138**, 117-135.

Och, L.M., Cremonese, L., Shields‐Zhou, G.A., Poulton, S.W., Struck, U., Ling, H., Li, D., Chen, X., Manning, C. and Thirlwall, M. (2015) Palaeoceanographic controls on spatial redox distribution over the Yangtze Platform during the Ediacaran–Cambrian transition. *Sedimentology* **63**, 378-410.

Och, L.M. and Shields-Zhou, G.A. (2012) The Neoproterozoic oxygenation event: environmental perturbations and biogeochemical cycling. *Earth Sci. Rev.* **110**, 26-57.

Och, L.M., Shields-Zhou, G.A., Poulton, S.W., Manning, C., Thirlwall, M.F., Li, D., Chen, X., Ling, H., Osborn, T. and Cremonese, L. (2013) Redox changes in Early Cambrian black shales at Xiaotan section, Yunnan Province, South China. *Precambrian Res.* **225**, 166-189.

Papineau, D., Purohit, R., Goldberg, T., Pi, D., Shields, G.A., Bhu, H., Steele, A. and Fogel, M.L. (2009) High primary productivity and nitrogen cycling after the Paleoproterozoic phosphogenic event in the Aravalli Supergroup, India. *Precambrian Res.* **171**, 37–56.

Pennock, J.R., Velinsky, D.J., Ludlam, J.M., Sharp, J.H. and Fogel, M.L. (1996) Isotopic fractionation of ammonium and nitrate during uptake by Skeletonema costatum: Implications for $\delta^{15}N$ dynamics under bloom conditions. *Limnol. Oceanogr.* **41**, 451-459.

Prokopenko, M., Hammond, D., Berelson, W., Bernhard, J., Stott, L. and Douglas, R. (2006) Nitrogen cycling in the sediments of Santa Barbara basin and Eastern Subtropical North Pacific: Nitrogen isotopes, diagenesis and possible chemosymbiosis between two lithotrophs (Thioplocaand Anammox) —"riding on a glider". *Earth Planet. Sci. Lett.* **242**, 186-204.

Reinhard, C.T., Planavsky, N.J., Gill, B.C., Ozaki, K., Robbins, L.J., Lyons, T.W., Fischer, W.W., Wang, C., Cole, D.B. and Konhauser, K.O. (2016) Evolution of the global phosphorus cycle. *Nature* **541**, 386-389.

Robbins, L.J., Lalonde, S.V., Planavsky, N.J., Partin, C.A., Reinhard, C.T., Kendall, B., Scott, C., Hardisty, D.S., Gill, B.C. and Alessi, D.S. (2016) Trace elements at the intersection of marine biological and geochemical evolution. *Earth Sci. Rev.* **163**, 323-348.

Robinson, R.S., Kienast, M., Luiza Albuquerque, A., Altabet, M., Contreras, S., De Pol Holz, R., Dubois, N., Francois, R., Galbraith, E. and Hsu, T.C. (2012) A review of nitrogen isotopic alteration in marine sediments. *Paleoceanography* **27**, 89-108.

Sahoo, S.K., Planavsky, N.J., Jiang, G., Kendall, B., Owens, J.D., Wang, X., Shi, X., Anbar, A.D. and Lyons, T.W. (2016) Oceanic oxygenation events in the anoxic Ediacaran ocean. *Geobiology* **14**, 457-468.

Saltzman, M.R., Young, S.A., Kump, L.R., Gill, B.C., Lyons, T.W. and Runnegar, B. (2011) Pulse of atmospheric oxygen during the late Cambrian. *Proc. Natl. Acad. Sci.* **108**, 3876-3881.

Sano, Y. and Pillinger, C.T. (2008) Nitrogen isotopes and N_2/Ar ratios in cherts. An attempt to measure time evolution of atmospheric $\delta^{15}N$ value. *Geochemical Journal* **24**, 315-325.

Schröder, S. and Grotzinger, J.P. (2007) Evidence for anoxia at the Ediacaran-Cambrian boundary: The record of redox-sensitive trace elements and rare earth elements in Oman. *Journal of the Geological Society* **164**, 175-187.

Schroeder, P.A. and Mclain, A.A. (1998) Illite-smectites and the influence of burial diagenesis on the geochemical cycling of nitrogen. *Clay Minerals* **33**, 539-546(538).

Scott, C., Lyons, T.W., Bekker, A., Shen, Y., Poulton, S.W., Chu, X. and Anbar, A.D. (2008) Tracing the stepwise oxygenation of the Proterozoic ocean. *Nature* **452**, 456-459.

Shu, D., Isozaki, Y., Zhang, X., Han, J. and Maruyama, S. (2014) Birth and early evolution of metazoans. *Gondwana Res.* **25**, 884-895.

Siebert, C., Kramers, J.D., Meisel, T., Morel, P. and Nägler, T.F. (2005) PGE, Re-Os, and Mo isotope systematics in Archean and early Proterozoic sedimentary systems as proxies for redox conditions of the early Earth. *Geochim. Cosmochim. Acta* **69**, 1787-1801.

Sigman, D.M., Altabet, M.A., Mccorkle, D.C., Francois, R. and Fischer, G. (2000) The $\delta^{15}N$ of nitrate in the southern ocean: Consumption of nitrate in surface waters. *Global Biogeochem. Cycles* **13**, 1149–1166.

Sigman, D.M., Karsh, K.L. and Casciotti, K.L. (2009) Ocean process tracers: nitrogen isotopes in the ocean. *Encyclopedia of ocean science*, 40-54.

Sohm, J.A., Webb, E.A. and Capone, D.G. (2011) Emerging patterns of marine nitrogen fixation. *Nature Reviews Microbiology* **9**, 499.

Somes, C.J., Schmittner, A., Galbraith, E.D., Lehmann, M.F., Altabet, M.A., Montoya, J.P., Letelier, R.M., Mix, A.C., Bourbonnais, A. and Eby, M. (2010) Simulating the global distribution of nitrogen isotopes in the ocean. *Global Biogeochem. Cycles* **24**, GB4019.

Sørensen, J. (1978) Capacity for denitrification and reduction of nitrate to ammonia in a coastal marine sediment. *Appl. Environ. Microbiol.* **35**, 301-305.

Sperling, E.A., Wolock, C.J., Morgan, A.S., Gill, B.C., Kunzmann, M., Halverson, G.P., Macdonald, F.A., Knoll, A.H. and Johnston, D.T. (2015) Statistical analysis of iron geochemical data suggests limited late Proterozoic oxygenation. *Nature* **523**, 451-454.

Steiner, M., Li, G., Qian, Y., Zhu, M. and Erdtmann, B.D. (2007) Neoproterozoic to Early Cambrian small shelly fossil assemblages and a revised biostratigraphic correlation of the Yangtze Platform (China). *Palaeogeogr. Palaeoclimatol. Palaeoecol.* **254**, 67-99.

Steiner, M., Zhu, M., Zhao, Y. and Erdtmann, B.D. (2005) Lower Cambrian Burgess Shale-type fossil associations of South China. *Palaeogeogr. Palaeoclimatol. Palaeoecol.* **220**, 129-152.

Stüeken, E.E. (2013) A test of the nitrogen-limitation hypothesis for retarded eukaryote radiation: Nitrogen isotopes across a Mesoproterozoic basinal profile. *Geochim. Cosmochim. Acta* **120**, 121-139.

Stüeken, E.E., Buick, R. and Schauer, A.J. (2015) Nitrogen isotope evidence for alkaline lakes on late Archean continents. *Earth Planet. Sci. Lett.* **411**, 1-10.

Stüeken, E.E., Kipp, M.A., Koehler, M.C. and Buick, R. (2016) The evolution of Earth's biogeochemical nitrogen cycle. *Earth Sci. Rev.* **160**, 220-239.

Talbot, M.R. and Johannessen, T. (1992) A high resolution palaeoclimatic record for the last 27,500 years in tropical West Africa from the carbon and nitrogen isotopic composition of lacustrine organic matter. *Earth Planet. Sci. Lett.* **110**, 23-37.

Tan, J., Horsfield, B., Mahlstedt, N., Zhang, J., Boreham, C.J., Hippler, D., van Graas, G. and Tocher, B.A. (2015) Natural gas potential of Neoproterozoic and lower Palaeozoic marine shales in the Upper Yangtze Platform, South China: geological and organic geochemical characterization. *International Geology Review* **57**, 305-326.

Tesdal, J.-E., Galbraith, E. and Kienast, M. (2013) Nitrogen isotopes in bulk marine sediment: linking seafloor observations with subseafloor records. *Biogeosciences* **10**, 101-118.

Thomazo, C., Ader, M. and Philippot, P. (2011) Extreme ^{15}N-enrichments in 2.72-Gyr-old sediments: evidence for a turning point in the nitrogen cycle. *Geobiology* **9**, 107-120.

Thomazo, C. and Papineau, D. (2013) Biogeochemical Cycling of Nitrogen on the Early Earth. *Elements* **9**, 345-351.

Thunell, R.C., Sigman, D.M., Muller-Karger, F., Astor, Y. and Varela, R. (2004) Nitrogen isotope dynamics of the Cariaco Basin, Venezuela. *Global Biogeochem. Cycles* **18**, GB3001.

Tyrrell, T. (1999) The relative influences of nitrogen and phosphorus on oceanic primary production. *Nature* **400**, 525-531.

Vo, J., Inwood, W., Hayes, J.M. and Kustu, S. (2013) Mechanism for nitrogen isotope fractionation during ammonium assimilation by Escherichia coli K12. *Proc. Natl. Acad. Sci.* **110**, 8696.

Wallace, M.W., Hood, A.v., Shuster, A., Greig, A., Planavsky, N.J. and Reed, C.P. (2017) Oxygenation history of the Neoproterozoic to early Phanerozoic and the rise of land plants. *Earth Planet. Sci. Lett.* **466**, 12-19.

Wang, D., Ling, H.-F., Struck, U., Zhu, X.-K., Zhu, M., He, T., Yang, B., Gamper, A. and Shields, G.A. (2018a) Coupling of ocean redox and animal evolution during the Ediacaran-Cambrian transition. *Nature Communications* **9**, 2575.

Wang, D., Struck, U., Ling, H.-F., Guo, Q.-J., Shields-Zhou, G.A., Zhu, M.-Y. and Yao, S.-P. (2015) Marine redox variations and nitrogen cycle of the early Cambrian southern margin of the Yangtze Platform, South China: Evidence from nitrogen and organic carbon isotopes. *Precambrian Res.* **267**, 209-226.

Wang, J., Chen, D., Yan, D., Wei, H. and Xiang, L. (2012a) Evolution from an anoxic to oxic deep ocean during the Ediacaran–Cambrian transition and implications for bioradiation. *Chem. Geol.* **s306–307**, 129-138.

Wang, J. and Li, Z.X. (2003) History of Neoproterozoic rift basins in South China: implications for Rodinia break-up. *Precambrian Res.* **122**, 141-158.

Wang, W., Guan, C., Zhou, C., Peng, Y., Pratt, L.M., Chen, X., Chen, L., Chen, Z., Yuan, X. and Xiao, S. (2017) Integrated carbon, sulfur, and nitrogen isotope chemostratigraphy of the Ediacaran Lantian Formation in South China: Spatial gradient, ocean redox oscillation, and fossil distribution. *Geobiology* **15**, 552.

Wang, X., Jiang, G., Shi, X., Peng, Y. and Morales, D. (2018b) Nitrogen isotope constraints on the early Ediacaran ocean redox structure. *Geochim. Cosmochim. Acta* **240**, 220-235.

Wang, X., Shi, X., Jiang, G. and Zhang, W. (2012b) New U–Pb age from the basal Niutitang Formation in South China: Implications for diachronous development and condensation of stratigraphic units across the Yangtze platform at the Ediacaran–Cambrian transition. *Journal of Asian Earth Sciences* **48**, 1-8.

Wang, X. and Zhang, W. (2013) Nitrogen Isotope Evidence for Redox Variations at the Ediacaran-Cambrian Transition in South China. *J. Geol.* **121**, 489-502.

Ward, B.A., Dutkiewicz, S. and Follows, M.J. (2014) Modelling spatial and temporal patterns in size-structured marine plankton communities: top–down and bottom–up controls. *Journal of Plankton Research* **36**, 31-47.

Ward, B.B., Devol, A.H., Rich, J.J., Chang, B.X., Bulow, S.E., Naik, H., Pratihary, A. and Jayakumar, A. (2009) Denitrification as the dominant nitrogen loss process in the Arabian Sea. *Nature* **461**, 78-81.

Wasmund, N., Voss, M. and Lochte, K. (2001) Evidence of nitrogen fixation by non-heterocystous cyanobacteria in the Baltic Sea and re-calculation of a budget of nitrogen fixation. *Marine Ecology Progress* **214**, 1-14.

Wei, G.-Y., Ling, H.-F., Li, D.A., Wei, W.E.I., Wang, D.A.N., Chen, X.I., Zhu, X.-K., Zhang, F.-F. and Yan, B.I.N. (2017) Marine redox evolution in the early Cambrian Yangtze shelf margin area: evidence from trace elements, nitrogen and sulphur isotopes. *Geol. Mag.* **154**, 1344-1359.

Wille, M., Kramers, J.D., Nägler, T.F., Beukes, N.J., Schröder, S., Meisel, T., Lacassie, J.P. and Voegelin, A.R. (2007) Evidence for a gradual rise of oxygen between 2.6 and 2.5 Ga from Mo isotopes and Re-PGE signatures in shales.

Geochim. Cosmochim. Acta **71**, 2417-2435.

Xiang, L., Schoepfer, S.D., Shen, S.-Z., Cao, C.-Q. and Zhang, H. (2017) Evolution of oceanic molybdenum and uranium reservoir size around the Ediacaran–Cambrian transition: Evidence from western Zhejiang, South China. *Earth Planet. Sci. Lett.* **464**, 84-94.

Xiang, L., Schoepfer, S.D., Zhang, H., Cao, C.-q. and Shen, S.-z. (2018) Evolution of primary producers and productivity across the Ediacaran-Cambrian transition. *Precambrian Res.* **313**, 68-77.

Xu, L., Lehmann, B., Mao, J., Qu, W. and Du, A. (2011) Re-Os Age of Polymetallic Ni-Mo-PGE-Au Mineralization in Early Cambrian Black Shales of South China--A Reassessment. *Econ. Geol.* **106**, 511-522.

Yang, A., Zhu, M. and Zhang, J. (2008) Chronostratigraphy of Cambrian Huangboling and Hetang Formations in Southern Anhui and Western Zhejiang. *Journal of Stratigraphy* **32**, 343-353.

Yang, A., Zhu, M., Zhang, J. and Li, G. (2003) Early Cambrian eodiscoid trilobites of the Yangtze Platform and their stratigraphic implications. *Progress in Natural Science: Materials International* **13**, 861-866.

Yang, B., Steiner, M., Li, G. and Keupp, H. (2014) Terreneuvian small shelly faunas of East Yunnan (South China) and their biostratigraphic implications. *Palaeogeogr. Palaeoclimatol. Palaeoecol.* **398**, 28-58.

Yang, C., Zhu, M., Condon, D.J. and Li, X.H. (2017) Geochronological constraints on stratigraphic correlation and oceanic oxygenation in Ediacaran-Cambrian transition in South China. *Journal of Asian Earth Sciences* **140**, 75-81.

Yang, X., Zhu, M., Guo, Q. and Zhao, Y. (2007) Organic Carbon Isotopic Evolution during the Ediacaran-Cambrian Transition Interval in Eastern Guizhou, South China: Paleoenvironmental and Stratigraphic Implications. *Acta Geologica Sinica* **81**, 194-203.

Yeasmin, R., Chen, D., Fu, Y., Wang, J., Guo, Z. and Guo, C. (2016) Climatic-oceanic forcing on the organic accumulation across the shelf during the Early Cambrian (Age 2 through 3) in the mid-upper Yangtze Block, NE Guizhou, South China. *Journal of Asian Earth Sciences* **134**, 365-386.

Yuan, Y., Cai, C., Wang, T., Xiang, L., Jia, L. and Chen, Y. (2014) Redox condition during Ediacaran-Cambrian transition in the Lower Yangtze deep water basin, South China: constraints from iron speciation and $\delta^{13}C_{org}$ in the Diben section, Zhejiang. *Science Bulletin* **59**, 3638-3649.

Zerkle, A.L., Junium, C.K., Canfield, D.E. and House, C.H. (2008) Production of N-depleted biomass during cyanobacterial N-fixation at high Fe concentrations. *J. Geophys. Res.: Biogeosci.* **113**, 112-118.

Zhai, L., Wu, C., Ye, Y., Zhang, S. and An, Z. (2016) Marine redox variations during the Ediacaran–Cambrian transition on the Yangtze Platform, South China. *Geol. J.* **53**, 58-79.

Zhai, L., Wu, C., Ye, Y., Zhang, S. and Wang, Y. (2018) Fluctuations in chemical weathering on the Yangtze Block during the Ediacaran–Cambrian transition: Implications for paleoclimatic conditions and the marine carbon cycle. *Palaeogeogr. Palaeoclimatol. Palaeoecol.* **490**, 280-292.

Zhang, J., Fan, T., Zhang, Y., Lash, G.G., Li, Y. and Wu, Y. (2017) Heterogenous oceanic redox conditions through the Ediacaran-Cambrian boundary limited the metazoan zonation. *Scientific Reports* **7**, 8550.

Zhang, S., Evans, D.A.D., Li, H., Wu, H., Jiang, G., Dong, J., Zhao, Q., Raub, T.D. and Yang, T. (2013) Paleomagnetism of the late Cryogenian Nantuo Formation and paleogeographic implications for the South China Block. *Journal of Asian Earth Sciences* **72**, 164-177.

Zhang, S., Li, H., Jiang, G., Evans, D.A.D., Dong, J., Wu, H., Yang, T., Liu, P. and Xiao, Q. (2015) New paleomagnetic results from the Ediacaran Doushantuo Formation in South China and their paleogeographic implications. *Precambrian Res.* **259**, 130-142.

Zhang, X., Sigman, D.M., Morel, F.M. and Kraepiel, A.M. (2014) Nitrogen isotope fractionation by alternative nitrogenases and past ocean anoxia. *Proc. Natl. Acad. Sci.* **111**, 4782-4787.

Zheng, Y.-F., Wu, R.-X., Wu, Y.-B., Zhang, S.-B. and Yuan, H. (2008) Rift melting of juvenile arc-derived crust: Geochemical evidence from Neoproterozoic volcanic and granitic rocks in the Jiangnan Orogen, South China. *Precambrian Res.* **163**, 351-383.

Zhou, C., Huyskens, M.H., Lang, X., Xiao, S. and Yin, Q.-Z. (2019) Calibrating the terminations of Cryogenian global

glaciations. *Geology* **251**, 251-254.

Zhou, C., Xie, G., McFadden, K., Xiao, S. and Yuan, X. (2007) The diversification and extinction of Doushantuo-Pertatataka acritarchs in South China: causes and biostratigraphic significance. *Geol. J.* **42**, 229-262.

Zhou, C., Zhang, J., Li, G. and Yu, Z. (1997) Carbon and oxygen isotopic record of the early cambrian from the Xiaotan section, Yunnan, South China. *Scientia Geologica Sinica* **32**, 201-211.

Zhou, M.Z., Luo, T.Y., Liu, S.R., Qian, Z.K. and Xing, L.C. (2013) SHRIMP zircon age for a K-bentonite in the top of the Laobao Formation at the Pingyin section, Guizhou, South China. *Science China Earth Sciences* **56**, 1677-1687.

Zhu, M., Gehling, J.G., Xiao, S., Zhao, Y. and Droser, M.L. (2008) Eight-armed Ediacara fossil preserved in contrasting taphonomic windows from China and Australia. *Geology* **36**, 867-870.

Zhu, M., Strauss, H. and Shields, G.A. (2007a) From snowball earth to the Cambrian bioradiation: Calibration of Ediacaran–Cambrian earth history in South China. *Palaeogeogr. Palaeoclimatol. Palaeoecol.* **254**, 1-6.

Zhu, M., Zhang, J. and Yang, A. (2007b) Integrated Ediacaran (Sinian) chronostratigraphy of South China. *Palaeogeogr. Palaeoclimatol. Palaeoecol.* **254**, 7-61.

Zhu, M., Zhang, J., Yang, A., Li, G., Steiner, M. and Erdtmann, B.D. (2003) Sinian-Cambrian stratigraphic framework forshallow-to deep-water environments of the Yangtze Platform: an integrated approach. *Progress in Natural Science* **13**, 951-960.

Zhu, M.Y. (2010) The origin and Cambrian explosion of animals: Fossil evidence from China. *Acta Palaeontologica Sinica* **49**, 269-287 (in Chinese with English abstract).

Zhu, M.Y., Yang, A.H., Yuan, J.L., Li, G.X., Zhang, J.M., Zhao, F.C., Ahn, S.Y. and Miao, L.Y. (2019) Cambrian integrative stratigraphy and timescale of China. *Science China Earth Sciences* **62**, 25-60.

Zhu, R.X., Li, X.H., Hou, X.G., Pan, Y.X., Wang, F., Deng, C.L. and He, H.Y. (2009) SIMS U-Pb zircon age of a tuff layer in the Meishucun section, Yunnan, southwest China: Constraint on the age of the Precambrian-Cambrian boundary. *Science in China* **52**, 1385-1392.

Figure Captions

Figure 1. The biogeochemical nitrogen cycle (adapted from Ader et al., 2016; Sigman et al., 2009; and Stüeken et al., 2016). Elements in parentheses are used as co-factors in enzymes and ε is the fractionation factor (‰) related to the metabolic process ($\varepsilon \approx \delta^{15}N_{product} - \delta^{15}N_{reactant}$).

Figure 2. Geological background and stratigraphic column for the studied drill core zk2012. A: Global paleogeographic map at 635–510 Ma (revised from Zhang et al., 2013, 2015). B: Paleogeographic map of Yangtze Block during the Ediacaran-Cambrian transition (after Yeasmin et al., 2016). Numbers in the maps indicate the locations of drill core zk2012 (No.7) and other reported sections discussed in the paper. C: Lithological column of the studied drill core zk2012. F-2 = Fortunian-Stage2 and NT = Nantuo Formation.

Figure 3. Chemostratigraphic profiles of TOC, TN, C_{org}/N, $\delta^{13}C_{org}$ and $\delta^{15}N_{bulk}$ for the studied drill core zk2012. The vertical

dashed line in the C_{org}/N profile denotes the Redfield ratio (C/N = 6.6). The horizontal dashed lines represent the bottom boundaries of Member I of Doushantuo Formation, Member II of Doushantuo Formation, Member III of Doushantuo Formation, Liuchapo Formation, early Cambrian, and Jiumenchong Formation, in ascending order.

Figure 4. A summary of regional chronostratigraphy, lithostratigraphy, biostratigraphy and the corresponding stratigraphic correlation in South China (revised from Steiner et al. 2007; Chen et al. 2015b; and Zhu et al. 2019). Radiometric ages are from previous studies (Condon et al., 2005; Compston et al., 2008; Chen et al., 2009; Jiang et al., 2009; Zhu et al., 2009; Xu et al., 2011; Wang et al., 2012b; Zhou et al., 2013; Chen et al., 2015a; Yang et al., 2017; Zhou et al., 2019). Fm. = Formation. Mb. = Member. Ass. = Assemblage.

Figure 5. Chemostratigraphic $\delta^{15}N_{bulk}$ profiles across the Yangtze Block during the Ediacaran-Cambrian transition. For the Yangtze Gorges composite section, the gray and black data are derived from Cremonese et al. (2013b) and Kikumoto et al. (2014), respectively. The three horizontal dashed lines represent lower boundaries of the late Ediacaran, Cambrian Fortunian, and Cambrian Stage 3 in ascending order. The red dashed line denotes the Ni–Mo–PGE-rich horizon. The simplified cross section of the Yangtze Block is based on the paleogeographic map in Fig. 2B. Sources of litho- and bio-stratigraphic data: 1) Xiaotan (XT): Intrashelf Basin (Zhou et al., 1997; Li, 2004; Steiner et al., 2007; Cremonese et al., 2013a; Och et al., 2013; Yang et al., 2014); 2) Yangtze-Gorges (YG): Intrashelf Basin (Chen, 1984; Steiner et al., 2007; Cremonese et al., 2013b; Guo et al., 2014; Kikumoto et al., 2014); 3) Zhongnan (ZN): Rimmed carbonate Platform (Steiner et al., 2005; Cremonese et al., 2013b; Och et al., 2013; Zhang et al., 2017); 4) Sancha (SC): Rimmed carbonate platform (Zhu et al., 2003; Steiner et al., 2005; Steiner et al., 2007; Li et al., 2012); 5) Nangao (NG): Slope (Yang et al., 2007; Zhang et al., 2017); 6) Huanglian/Daotuo (HL/DT): Slope (Zhu et al., 2003; Cremonese et al., 2013b; Wei et al., 2017); 7) zk2012: Slope (This study); 8) Longbizui (LBZ): Lower slope (Wang et al., 2012a; Cremonese et al., 2013b; Guo et al., 2013; Guo et al., 2016); 9) Lijiatuo (LJT): Lower slope (Guo et al., 2007; Cremonese et al., 2013b); 10) Yanjia/Lantian (YaJ/LT): Lower slope (Wang et al., 2017; Wang et al., 2018a); 11) Yuanjia (YuJ): Basin (Wang et al., 2015).

Figure 6. Cross plots of (a) TOC versus TN, (b) $\delta^{15}N_{bulk}$ versus TN, (c) $\delta^{15}N_{bulk}$ versus C_{org}/N, (d) $\delta^{15}N_{bulk}$ versus TOC, (e) $\delta^{15}N_{bulk}$ versus $\delta^{13}C_{org}$, and (f) $\delta^{13}C_{org}$ versus TOC. Trend lines and correlation coefficients are presented for each formation/lithology in each cross plot.

Figure 7. a. Distribution of nitrogen isotope data from drill core zk2012 and previous studied sections (Cremonese et al., 2013a; Cremonese et al., 2013b; Ader et al., 2014; Kikumoto et al., 2014; Wang et al., 2015; Wang et al., 2017; Wei et al., 2017; Zhang et al., 2017; Wang et al., 2018a) deposited on the Yangtze Block during the Ediacaran-Cambrian transitional period. The gray horizontal bars represent the range of $\delta^{15}N_{bulk}$ generated by Mo-contained N_2-fixation. b. Statistical analysis of $\delta^{15}N_{bulk}$ (‰) in Yangtze Block for four time bins (635Ma–551Ma; 551Ma–541Ma; 541Ma–522Ma; 522Ma–514Ma). The distribution of $\delta^{15}N_{bulk}$ is represented by the average values (red diamond) and standard deviations (± 1σ). Ed = Ediacaran, 2 = Stage 2, 3 = Stage 3.

Figure 8. Scatter plot of TOC versus TN for upper Liuchapo and Jiumenchong formations in zk2012 studied drill core.

Figure 9. Schematic representations of different N-cycles from the early Ediacaran to early Cambrian on the Yangtze Block. The red dashed lines represent the redoxcline.

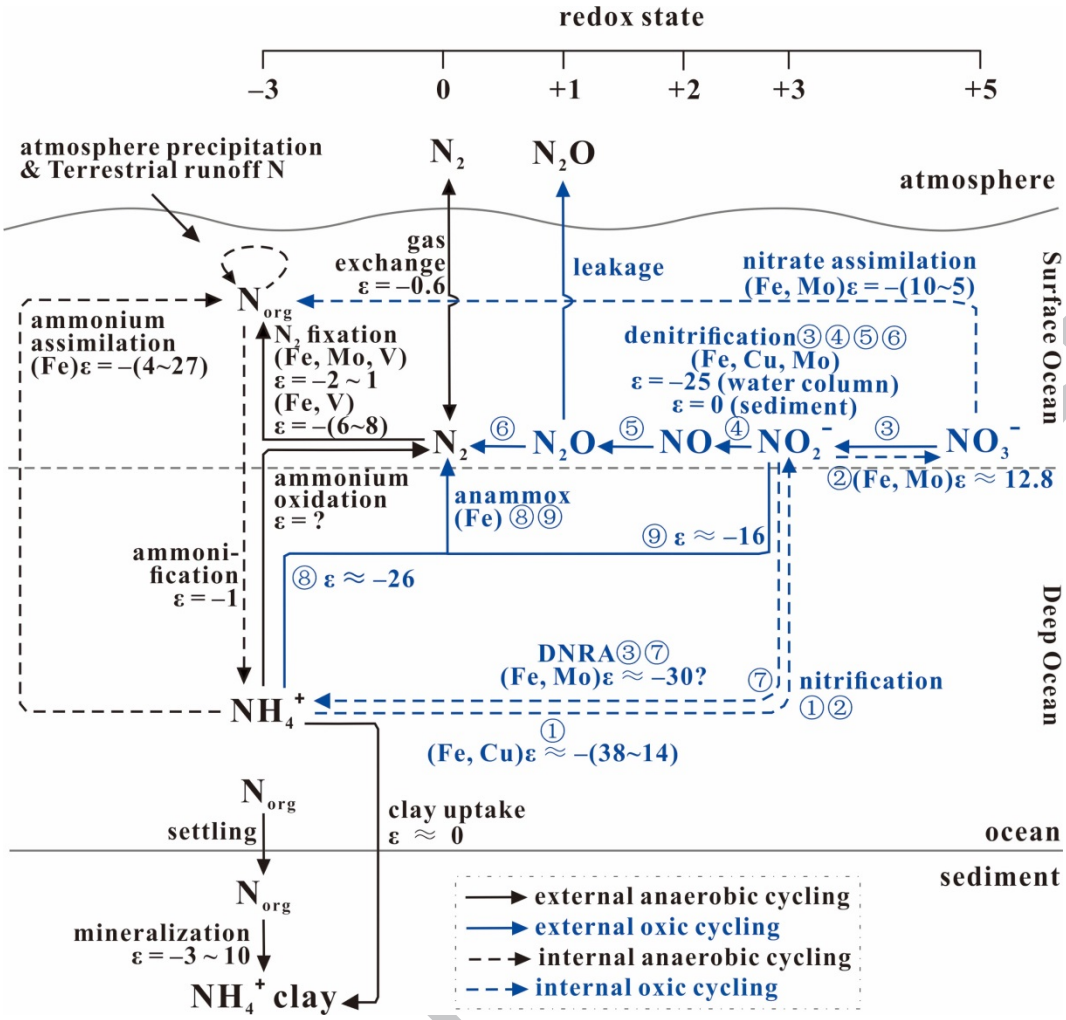

Figure 1

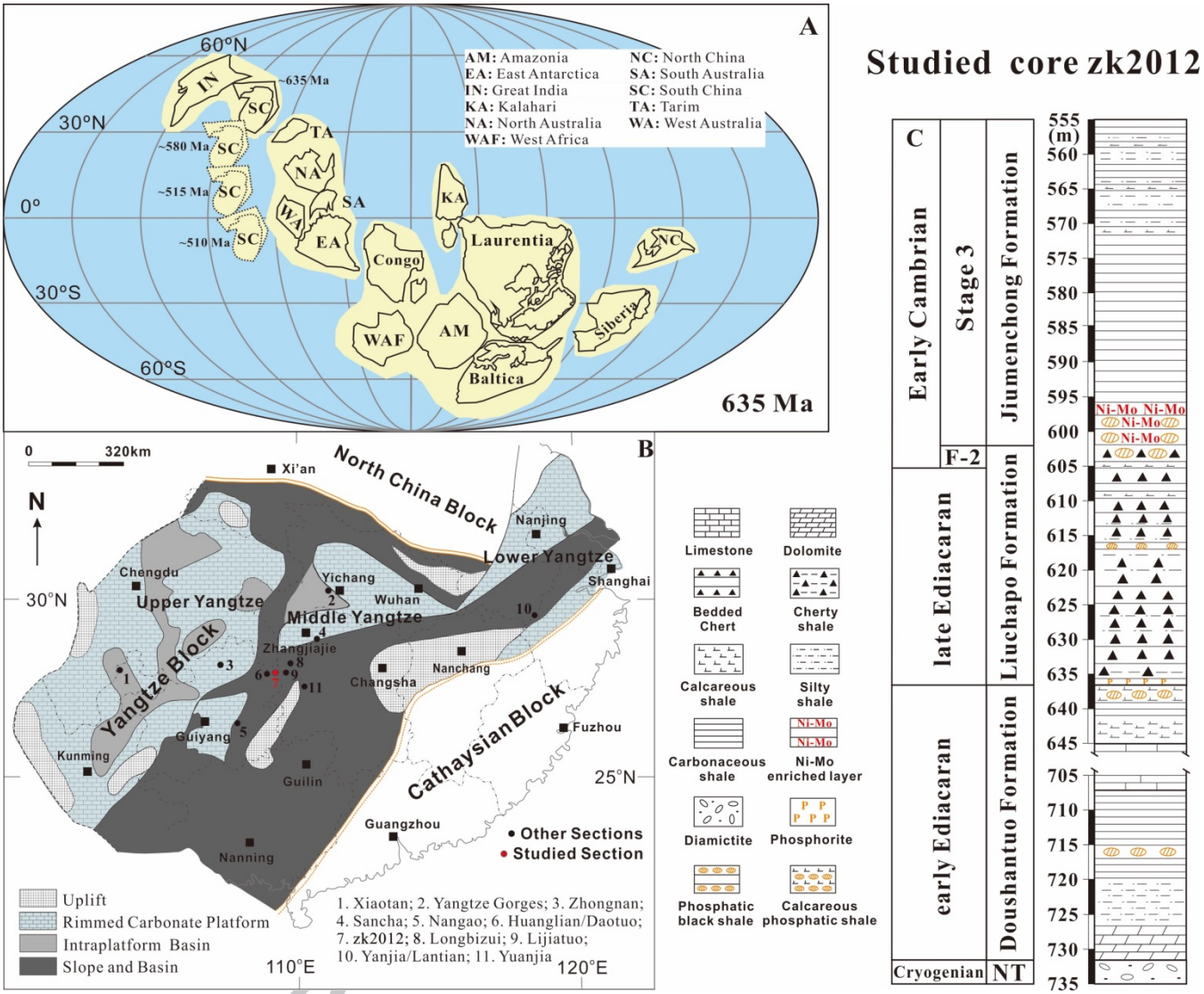

Figure 2

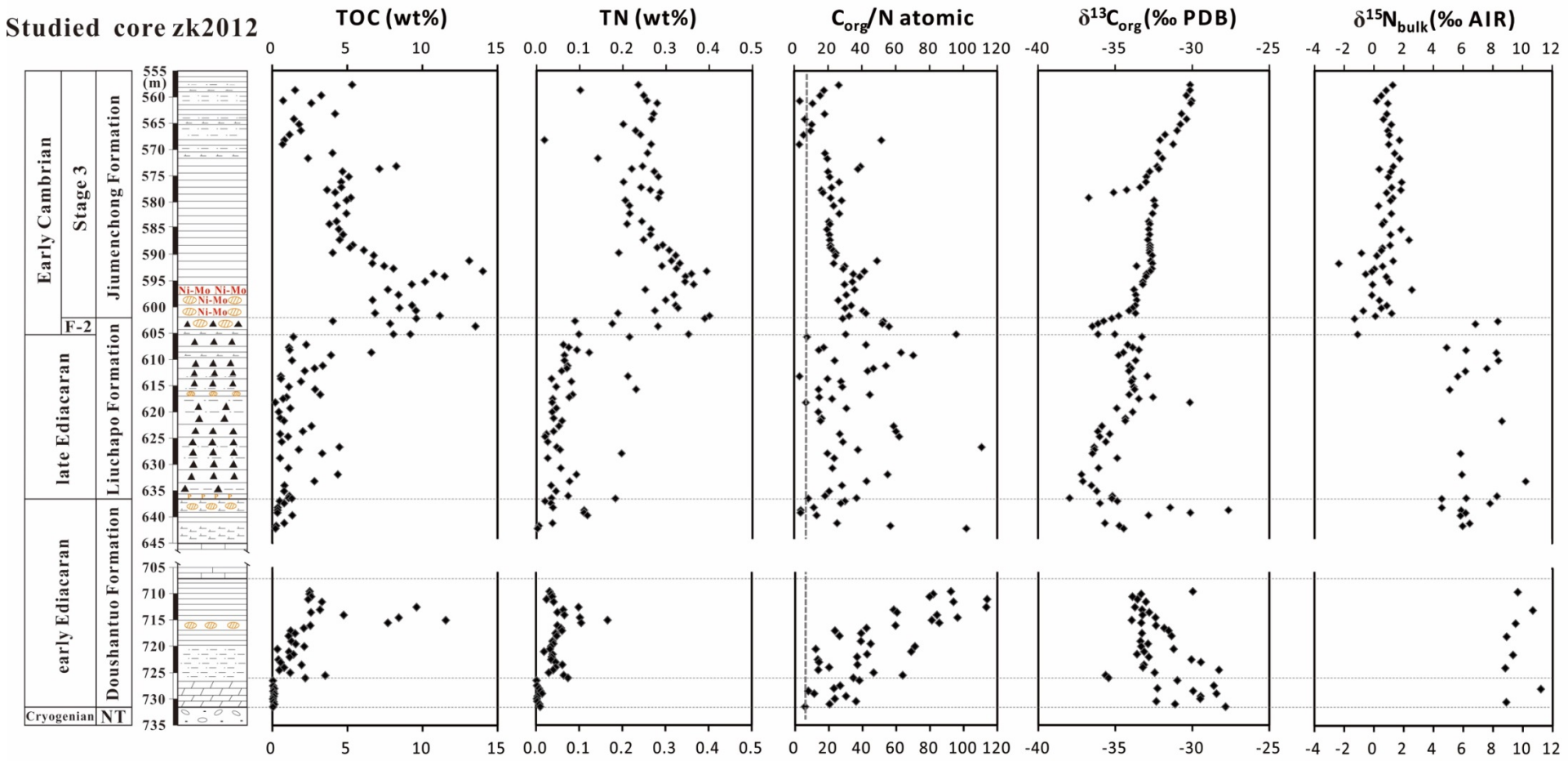

Figure 3

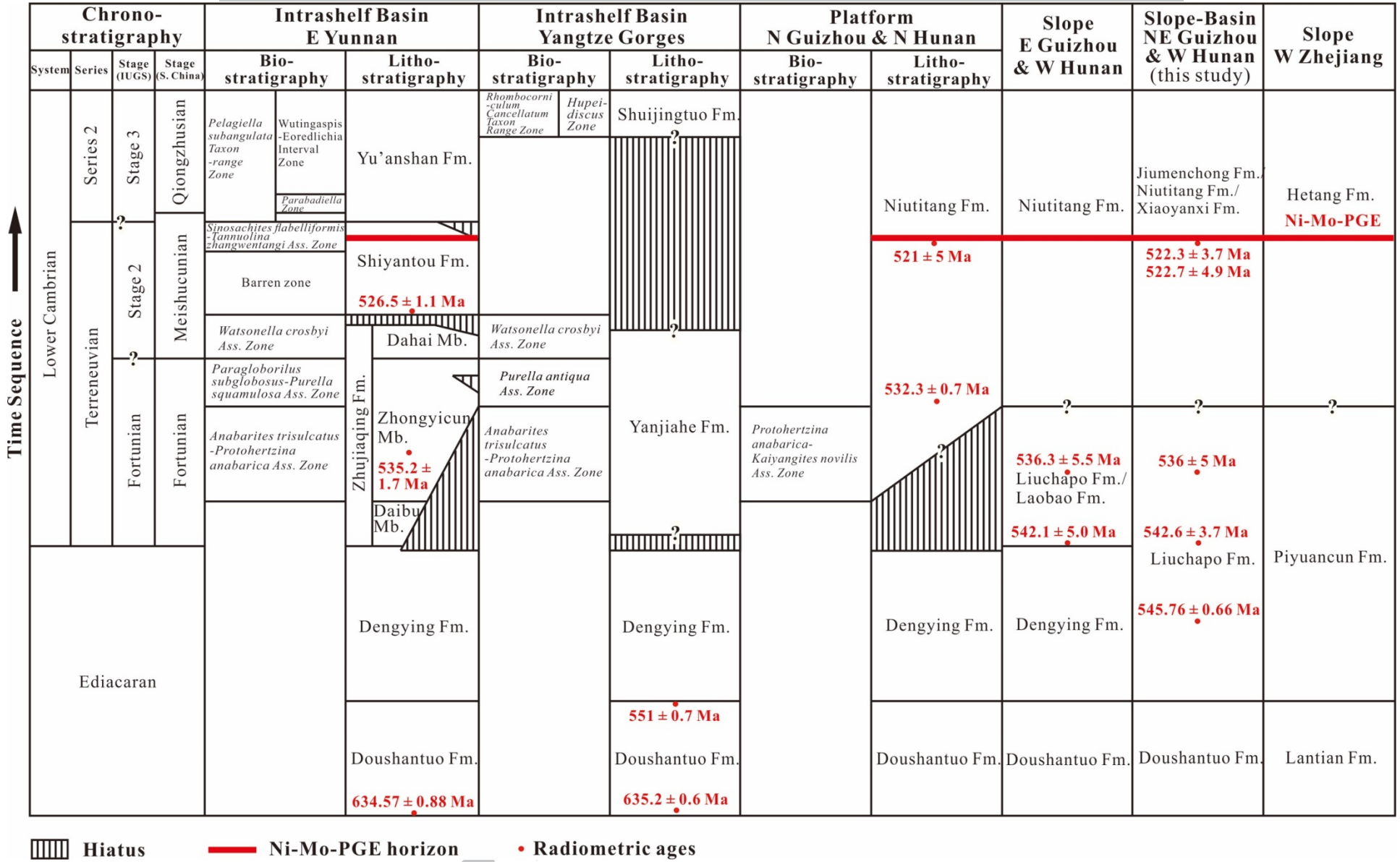

Figure 4

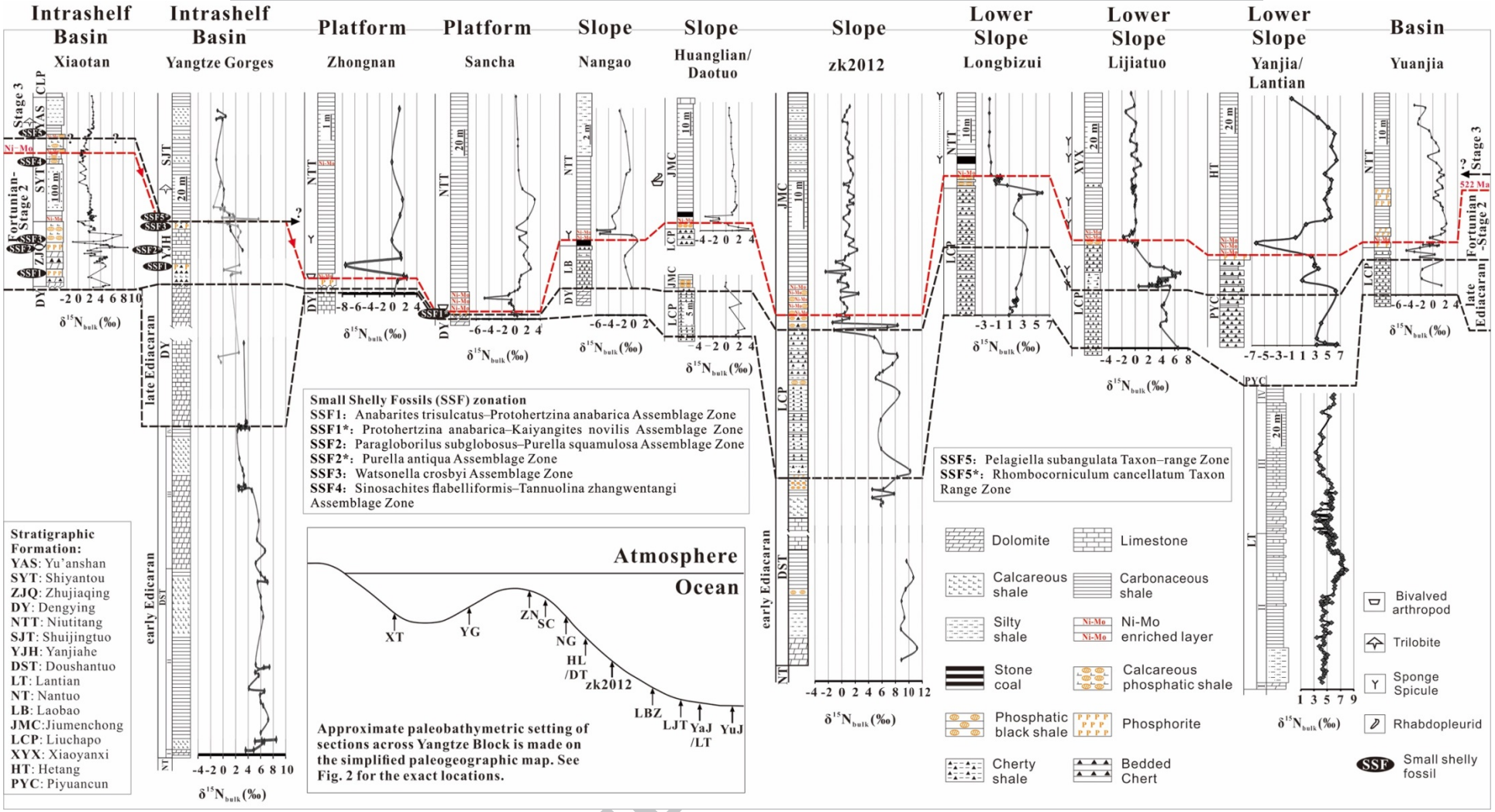

Figure 5

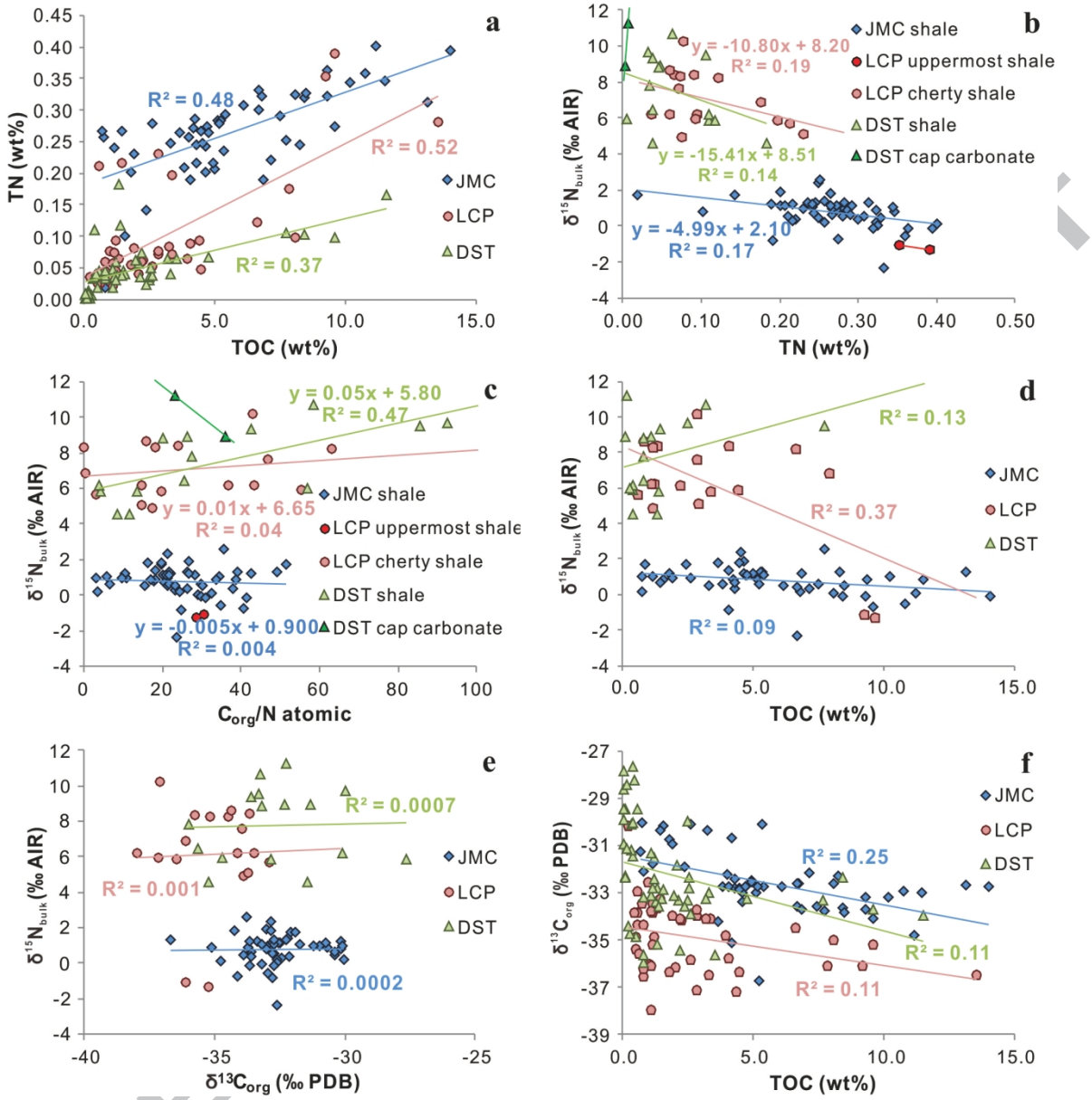
a
TN (wt%)
TOC (wt%)
R² = 0.48
R² = 0.52
R² = 0.37
JMC
LCP
DST
b
δ15Nbulk (‰ AIR)
TN (wt%)
y = -10.80x + 8.20
R² = 0.19
y = -15.41x + 8.51
R² = 0.14
y = -4.99x + 2.10
R² = 0.17
JMC shale
LCP uppermost shale
LCP cherty shale
DST shale
DST cap carbonate
c
δ15Nbulk (‰ AIR)
Corg/N atomic
y = 0.05x + 5.80
R² = 0.47
y = 0.01x + 6.65
R² = 0.04
y = -0.005x + 0.900
R² = 0.004
JMC shale
LCP uppermost shale
LCP cherty shale
DST shale
DST cap carbonate
d
δ15Nbulk (‰ AIR)
TOC (wt%)
R² = 0.13
R² = 0.37
R² = 0.09
JMC
LCP
DST
e
δ15Nbulk (‰ AIR)
δ13Corg (‰ PDB)
R² = 0.0007
R² = 0.001
R² = 0.0002
JMC
LCP
DST
f
δ13Corg (‰ PDB)
TOC (wt%)
R² = 0.25
R² = 0.11
R² = 0.11
JMC
LCP
DST

Figure 6

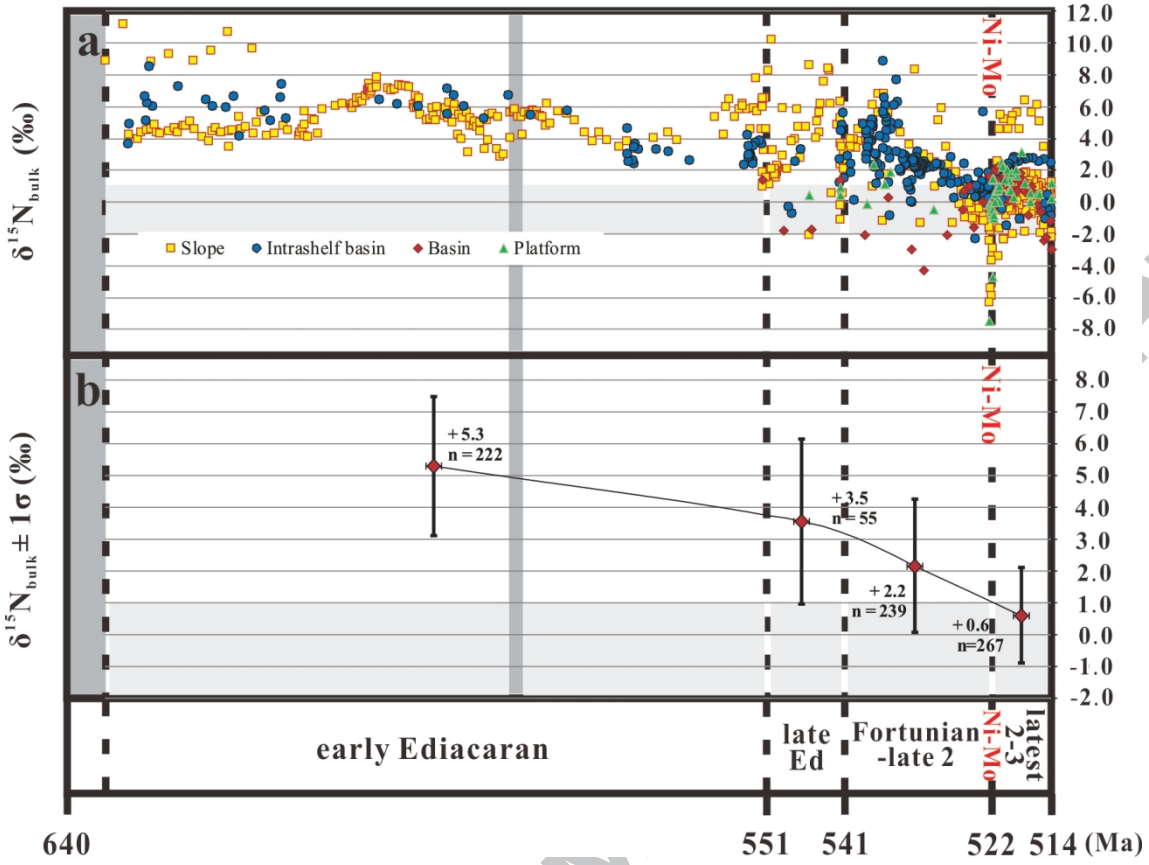

Figure 7

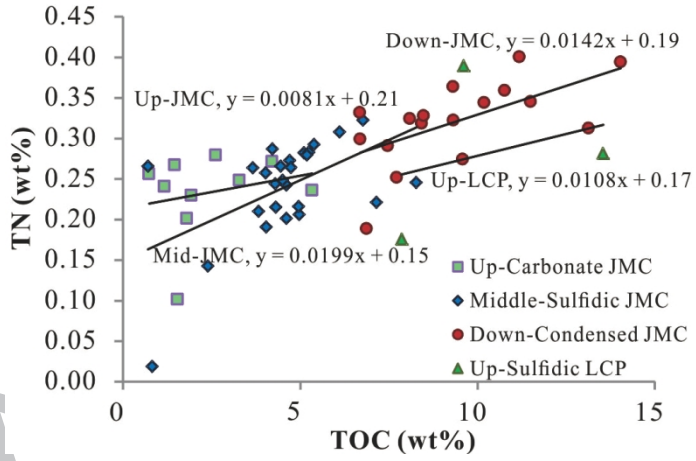

Figure 8

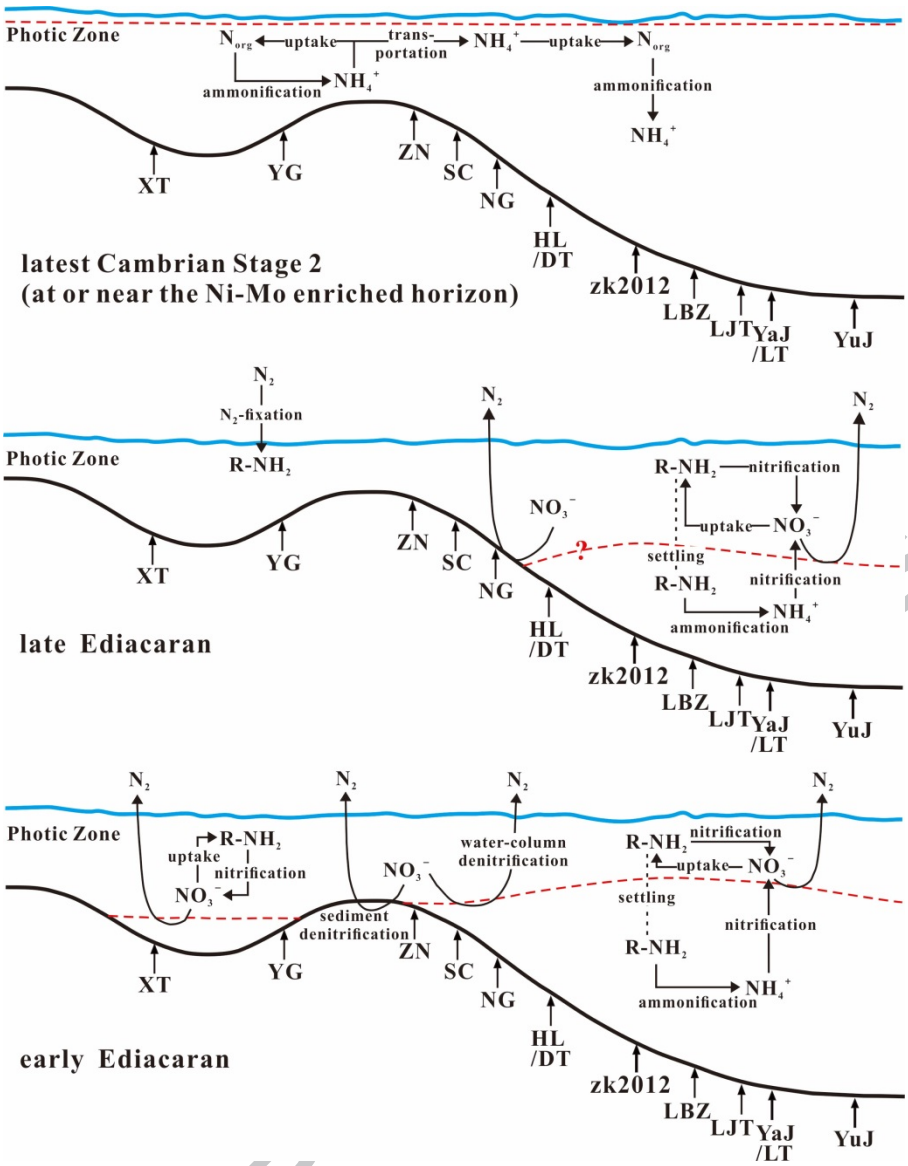

Figure 9

Table 1 Possible interpretations for sedimentary $\delta^{15}N$ values in the geological record

$\delta^{15}N$	Dominant metabolism in seawater	Examples
> 2‰	1. Assimilation of upwelled NO_3^- that experienced non-quantitative denitrification, Anammox or DNRA in the water column. 2. Assimilation of upwelled NH_4^+ that experienced non-quantitative nitrification. 3. Non-quantitative assimilation of upwelled NO_3^- or NH_4^+. 4. Assimilation of NH_4^+ that experienced partial NH_3 volatilization at high pH.	1. Eastern Tropical North Pacific (ETNP) (1); Eastern Tropical South Pacific (ETSP) (2); Arabian Sea (1). 2. Bering Sea (3); late Archean lakes (4). 3. Southern Ocean (5); Equatorial Pacific (6); no examples for NH_4^+ assimilation. 4. alkaline Lake Bosumtwi (7); late Archean alkaline lakes (8).
–2‰ ~ 1‰	1. Biological N_2-fixation with Mo-based nitrogenase. 2. Assimilation of NO_3^- from a wholly oxygenated ocean with denitrification only in sediments.	1. much of the open ocean (9); Black Sea (10); Cariaco Basin (11). 2. no examples.
< –2‰	1. Biological N_2-fixation with V- or Fe-based nitrogenases. 2. Non-quantitative assimilation of upwelled NH_4^+.	1. Cretaceous Oceanic Anoxic Events (OAEs) (12). 2. OAEs (13); late Paleoproterozoic (14).

Note: Ref. (1) Brandes et al. (1998), (2) Ward et al. (2009), (3) Morales et al. (2014), (4) Thomazo et al. (2011), (5) Sigman et al. (2000), (6) Somes et al. (2010), (7) Talbot and Johannessen (1992), (8) Stüeken et al. (2015), (9) Altabet (1988), (10) Fulton et al. (2012), (11) Haug et al. (1998), (12) Kuypers et al. (2004), (13) Higgins et al. (2012), (14) Papineau et al. (2009).